

Tuning Chemical Precompression: Theoretical Design and Crystal Chemistry of Novel Hydrides in the Quest for Warm and Light Superconductivity at Ambient Pressures

Katerina P. Hilleke¹ and Eva Zurek^{1, a)}

Department of Chemistry, State University of New York at Buffalo, Buffalo, NY 14260-3000, USA

Over the past decade, a combination of crystal structure prediction techniques and experimental synthetic work has thoroughly explored the phase diagrams of binary hydrides under pressure. The fruitfulness of this dual approach is demonstrated in the recent identification of several superconducting hydrides with T_c s approaching room temperature. We start with an overview of the computational procedures for predicting stable structures and estimating their propensity for superconductivity. A survey of phases with high T_c reveals some common structural features that appear conducive to the strong coupling of the electronic structure with atomic vibrations that leads to superconductivity. We discuss the stability and superconducting properties of phases containing two of these – molecular H_2 units mixed with atomic H and hydrogenic clathrate-like cages – as well as more unique motifs. Finally, we argue that ternary hydride phases, which are far less-explored, are a promising route to achieving simultaneously superconductivity at high temperatures and stability at low pressures. Several ternary hydrides arise from the addition of a third element to a known binary hydride structure through site mixing or onto a new site – and several more are based on altogether new structural motifs.

I. INTRODUCTION

Many diamonds have been broken, and CPU hours have been burned. Yet, at long last the elusive goal of high-temperature superconductivity in light element systems, as originally proposed by Ashcroft in 1968¹, is at hand. Record-breaking superconducting critical temperatures (T_c s) have been measured in a handful of exotic hydrides such as H_3S (203 K at 155 GPa)², LaH_{10} (250-260 K near 200 GPa)^{3,4}, YH_9 (240-260 K at 180-200 GPa^{5,6}), YH_6 (\sim 220 K at 165-185 GPa^{6,7}), and most notably a T_c of 288 K at 267 GPa has been reported in a C-S-H phase⁸. These materials defy classical chemical structure and bonding concepts, and challenge the notion that high T_c s are the domain of unconventional superconductors. In many cases, their discovery was theoretically inspired, contrary to Matthias' sixth rule for guiding a successful search for new superconducting materials, "Stay away from theorists!"⁹.

The obsession with squeezing hydrogen until it metallizes can be traced back to a 1926 proposal by J.D. Bernal. This idea was communicated in the literature for the first time by Wigner and Huntington, who proposed that at 25 GPa hydrogen, the first element of the periodic table, would follow its neighbors in group I to adopt a metallic solid structure^{10,11}. Ashcroft argued that in such a state the light mass of hydrogen, with its concomitant high phonon frequencies, large concentration of electronic states near the Fermi level, and strong electron phonon coupling arising from the lack of screening by core electrons would yield a superconducting phase that could maintain its character up to very high temperatures¹. At the time, the highest known T_c , of 18 K, was exhibited by the A15 intermetallic Nb_3Sn ¹², and it was overtaken in 1975 by the isotypic Nb_3Ge with T_c up to 22 K in sputtered thin films¹³ (Figure 1). Far from achieving superconductivity at room temperature, these T_c s did not even approach the boiling

point of nitrogen (77 K). Thus, the race to metallize hydrogen and harness its remarkable putative superconductivity was on.

For a while, it seemed as though a completely different family of materials, the superconducting cuprates, could be the first to break the room-temperature barrier, with a Y-Ba-Cu-O phase that possessed a T_c of 93 K being the first to surpass the boiling point of liquid nitrogen¹⁴. Unlike Nb_3Sn , Nb_3Ge , and the recently synthesized metal hydride superconductors, this family of materials belongs to a class of unconventional superconductors whose superconducting mechanism, though not fully understood, cannot be explained by Bardeen-Cooper-Schrieffer (BCS) theory.

Despite the continuing increase of the predicted pressure of hydrogen metallization^{15–20}, keeping elemental hydrogenic superconductivity just out of reach, a new strategy to lower the metallization pressure was proposed. Ashcroft suggested hydrogen dominant alloys as plausible candidates for achieving metallicity – and superconductivity – at lower pressures than elemental hydrogen, owing to the "chemical precompression" from the alloying element.²¹ The group 14 hydrides such as SiH_4 and GeH_4 were first suggested, in part because they possessed four completely occupied bands, similar to the recently discovered light-element conventional superconductor MgB_2 ²², as well as the propensity of the tetrrels towards superconductivity (albeit under pressure, in the case of Si and Ge).

A plethora of studies on the $Si-H$ ^{23–26} and $Ge-H$ ^{27,28} systems were promptly undertaken – including in the nascent field of *ab initio* crystal structure prediction (CSP), which has been shown to be useful in identifying a variety of stable and metastable structures. At elevated pressures where the chemical intuition of the ambient-pressure-trained minds of most scientists starts to fail^{29,30}, computational CSP techniques were especially helpful³¹. Not only are stoichiometries unimaginable at ambient pressure predicted to become stable, including $NaCl_7$ ³² and H_4I^{33} , but strange new structures comprised of curious motifs such as fused H_5 pentagons or clathrate-like cages composed of hydrogen can appear³⁴.

^{a)}Electronic mail: ezurek@buffalo.edu

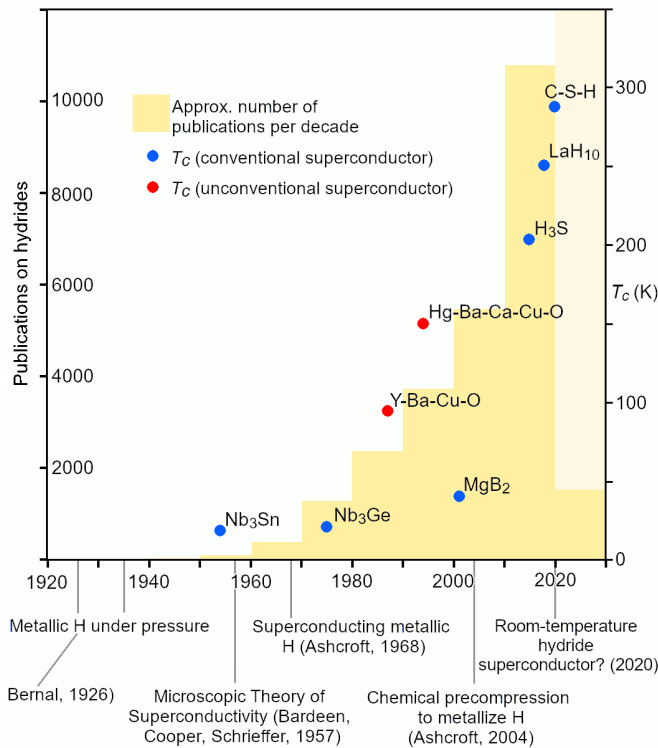


FIG. 1. Progress and interest in the field of superconducting hydrides over time. The approximate number of publications involving hydride superconductivity (left y-axis, yellow bars) has grown rapidly, with landmark publications highlighted below. Key experimentally measured T_c values (right y-axis, blue dots for conventional superconductors and red dots for unconventional superconductors) increase from modest temperatures in Nb_3Sn to near room-temperature superconductivity in the high pressure LaH_{10} and C-S-H phases.

Ultimately, this line of research resulted in the discovery of the hydride phases with record-breaking T_c s mentioned in our opening. But, much more work remains to be done! The remarkable superconducting properties emerge only at pressures approaching those experienced at the center of the Earth. Few high- T_c hydrides are predicted to remain stable at pressures below one megabar, and over the past decade most high-pressure binary hydride phase diagrams have already been exhaustively investigated.^{35,36} The same cannot be said for ternary phase diagrams. What’s more, it has been suggested that increasing complexity could result in phases that possess both high T_c s and the ability to be quenched to lower pressures. The latter property represents an extension of the chemical precompression idea: in the same way that a metal atom could “chemically precompress” pure hydrogen, stuffing a third element into a binary hydride might render it stable to lower pressures. The staggeringly vast phase space of ternary hydride materials is only beginning to be systematically explored, and it has been proposed that chemical concepts and machine-learning approaches will be useful in guiding such searches^{37–39}.

In this Perspective, we review superconductivity in hydrides stable at elevated pressures, with particular focus on the alkaline and rare earth metal binary hydride phases as well as on ternary hydride systems that can be constructed by alloying these binaries with another metal or a main group element. In section II we provide an overview of the computational techniques and methodologies employed in current computational studies of high-pressure hydrides, first covering *ab initio* crystal structure prediction, then the equations and procedures used to estimate T_c s. In section III we present the binary phases, grouping them into families based on structural motifs of the hydrogen sublattices – mixing of molecular and atomic hydrogen, clathrate-like cages, and additional curious motifs including fused H_5 pentagons. Ternary hydride materials ranging from substitutions of a third element into a binary hydride phase to altogether new structures are covered in Section IV, and we close with a brief outlook in Section V.

II. COMPUTATIONAL TECHNIQUES

A. Computational Methodologies

At the pressures required to stabilize many of the superconducting polyhydrides, the chemical intuition developed from living at atmospheric pressure breaks down. Seemingly bizarre stoichiometries such as NaCl_3 ³² and FeH_5 ⁴⁰ have been synthesized in diamond anvil cell experiments. Meanwhile, geometrical motifs that are not observed at 1 atm such as the pentagraphene units in ScH_{10} ²⁹ and HfH_{10} ⁴¹, as well as the hydrogenic clathrate cages in CaH_6 ⁴² and LaH_{10} ^{43,44} have been predicted. Pressure also influences the electronic structure and physical properties of matter. For example, in a behavior reversal, whereas hydrogen is expected to become metallic and superconducting,^{1,10,45} sodium undergoes a metal-to-insulator transition under pressure.⁴⁶

These are some of the reasons *a priori* CSP techniques have emerged as the methods of choice to identify promising synthetic targets computationally.^{31,47–49} What’s more, high pressure experiments may be difficult to execute, the products made can be challenging to characterize, the material properties hard to interrogate, and the results subject to interpretation. As computational techniques improve, CSP may become increasingly important in identifying synthetic targets for useful properties ranging from superhardness⁵⁰ to superconductivity⁵¹. Moreover, CSP is steadily gaining importance in helping to characterize already synthesized materials whose structures are unknown.

Several techniques for predicting global and important local minima of a crystalline material have been leveraged to great success. The global optimization schemes used towards this end are stochastic in nature, with no guarantee of finding the true global minimum within a potential energy surface (PES) that can be highly complex and contain several competitive local minima. The techniques that have been developed are thus based on several metaheuristics designed to find good solutions for optimization problems. These include minima hopping^{52–54}, simulated annealing⁵⁵, metadynamics^{56,57},

particle swarm optimization^{58,59}, genetic (evolutionary) algorithms^{60,61}, and (quasi-) random searches^{62,63}. Whereas the first three are best suited for local exploration, the latter three can broadly traverse the PES. Quantifying the performance of an algorithm is difficult due to their stochastic nature, however it has been shown that various options can greatly enhance the success rate⁶⁴.

Over the course of a CSP search, a single run can generate hundreds to thousands of structures. Often, multiple runs are required to ensure the global minimum has been found – and furthermore, CSP is often performed at various pressures. All of this is compounded by the fact that identification of stable phases requires generation of a full convex hull of a system. While some CSP techniques construct the convex hull on the fly, others require individual searches be performed for all chosen stoichiometries. Each of these thousands of structures is then optimized, typically using density functional theory (DFT), to the nearest stationary point. With the exception of dynamics based schemes, CSP explores the 0 K PES, as calculating the vibrational contributions to the free energy requires a significant increase in computational power relative to local relaxation.

Geometry optimizations are usually performed within DFT using the generalized gradient approximation (GGA) functional family, commonly that of Perdew, Burke, and Ernzerhof⁶⁵. Recently, some CSP techniques have employed machine learned interatomic potentials that can be parameterized via active learning, allowing for local optimizations to take place on greatly reduced timescales relative to DFT⁶⁶⁻⁶⁹, however, these are not yet widely implemented. On the other hand, complex electronic structures may necessitate the use of *meta*-GGA functionals such as SCAN⁷⁰ or treatment of dispersion⁷¹⁻⁷³. However, functionals that go beyond GGA are typically employed only to get a more accurate energy ordering after the CSP search is complete⁷⁴⁻⁷⁷, to manage computational expense. Since GGA-type functionals tend to underestimate metallization that results from pressure induced band broadening, hybrid functionals such as HSE06⁷⁸ are often employed to verify metallicity.

Structures of a similar composition are ranked by enthalpy (for high pressure calculations) or internal energy (for ambient pressure calculations). The relevant thermodynamic quantity is plotted versus composition to trace out the convex hull. The phases that lie on the hull are thermodynamically stable, but dynamic stability must also be checked by calculating phonon dispersions and confirming the absence of imaginary phonon modes. At this point, additional corrective factors to the hull can be considered, including the zero-point energy (ZPE) and the role of anharmonic effects. The latter is quite onerous to calculate, so it is typically neglected. However, it has been illustrated that anharmonic effects can alter the PES and superconducting properties of many of the high temperature superconducting hydrides⁷⁹⁻⁸¹. Meanwhile, the light mass and resultant high frequency atomic vibrations associated with hydrogen tend to culminate in substantial ZPE contributions. As a consequence, the inclusion of ZPE can alter the pressure range within which a given phase is stable, or stabilize one structure over another. Thus, ZPE effects are typically in-

cluded in final determinations of a convex hull or pressure-stability ranges of different structures.

Let us now summarize the computational workflow for the discovery of superconducting hydrides. After choosing a system for study, CSP runs at various pressures are carried out to find the most stable configurations as a function of composition. A number of the top candidates are chosen for a second round of local optimizations with higher accuracy settings, obtaining finalized lattices and enthalpies of formation. Calculations of phonon dispersions show which phases are dynamically stable and allow for the inclusion of ZPE into the 0 K enthalpy of formation. A convex hull is plotted – often with and without the ZPE – indicating which structures are expected to be stable (or low-lying metastable) at various pressures. Metastable phases are often reported because the real experimental conditions used for the synthesis can stabilize them. The following may guide the selection of structures to keep: a datamining analysis of the Materials Project database revealed that the median metastability (by DFT calculation) of all known inorganic crystalline materials was roughly 15 meV/atom, going up to roughly 70 meV/atom at the 90th percentile.⁸² The electronic structure of these phases is examined to determine which ones may have a large propensity for superconductivity (those with a high density of states at the Fermi level, DOS at E_F), and estimates of their T_c , using the techniques described in the next section, are made.

B. Calculating the Critical Temperature

In 1911, Onnes detected an abrupt disappearance in the resistivity of Hg metal at very low temperatures⁸³, sparking investigations into the cause of this phenomenon, termed superconductivity. An important hint came from the discovery of the isotope effect⁸⁴⁻⁸⁶, where the onset of superconductivity could be altered merely by the atomic mass of an element. This suggested that the vibrations of a crystalline lattice, which are dependent on atomic mass, may be important for the superconducting mechanism. In 1957, Bardeen, Cooper, and Schrieffer (BCS) published their *Microscopic Theory of Superconductivity*^{87,88}, describing the underlying theory for what are now known as conventional superconductors. These materials include intermetallic compounds such as Nb₃Sn¹² and MgB₂²², as well as the hydrogen-based materials we are concerned with here, such as H₃S^{2,89} and LaH₁₀^{3,43,44,90}.

BCS theory postulates that the coupling of the motion of an electron with a phonon can overcome the Coulomb repulsion between the two negatively charged particles, resulting in an electron pair that is a composite boson. Typically, this interaction is illustrated in the following scenario. As an electron moves within a crystalline lattice, the Coulombic attraction between the electron and the positive ion cores leads to a momentary distortion of the lattice towards the electron, resulting locally in a slightly higher positive charge. A second electron, with opposite spin and momentum to the first, is attracted to this region. At great distances, this attractive force can overcome the Coulombic repulsion between a pair of negatively charged electrons, resulting in a paired state termed a

Cooper pair. Although net attractive, this interaction between two electrons remains quite weak and can be broken with sufficient thermal energy. The critical temperature, T_c , marks the temperature above which the Cooper pairs are destroyed and the phase is no longer superconducting.

Within BCS theory T_c can be obtained via:

$$k_B T_c = 1.14 \hbar \omega \exp \left[\frac{-1}{N(0)V} \right] \quad (1)$$

where ω is the average phonon frequency of the system, $N(0)$ is the single spin DOS at E_F , and V is the pairing potential from the electron-phonon interaction. This expression, however, does not account for the damping effect in the electron-phonon interaction that arises because the displacements of the heavier ions associated with the phonon modes are slower than the motion of the light electrons.

To account for this, the Eliashberg equations⁹¹, based on a Green's function formalism, include the damping effect and can be solved numerically. A key quantity, termed the Eliashberg spectral function, $\alpha^2 F(\omega)$, can be computed via

$$\alpha^2 F(\omega) = \frac{1}{2\pi N(0)} \sum_{qj} \frac{\gamma_{qj}}{\omega_{qj}} \delta(\hbar\omega - \hbar\omega_{qj}), \quad (2)$$

with phonon linewidth, γ_{qj} , and frequency, ω_{qj} for a phonon j with a wavevector q .

McMillan performed numerical solution of the Eliashberg equations for 22 systems to determine a simple expression that could be used to estimate T_c ⁹². The phonon DOS of Nb was used to model the shape of the Eliashberg spectral function (Equation 2), yielding the simplified formula

$$T_c = \frac{\Theta_D}{1.45} \exp \left[- \frac{1.04(1 + \lambda)}{\lambda - \mu^*(1 + 0.62\lambda)} \right] \quad (3)$$

based on the Debye frequency, Θ_D , and the renormalized Coulomb repulsion parameter, μ^* . The electron-phonon coupling constant, λ , is derived from the Eliashberg spectral function according to

$$\lambda = 2 \int_0^\infty \frac{\alpha^2 F(\omega)}{\omega} d\omega. \quad (4)$$

In cases where the phonon spectrum of the system differed greatly from that of Nb – in Hg, for example – the electron phonon coupling (EPC) constant λ extracted from tunneling experiments differed from the value of λ obtained by solving Equation 3 given experimental values of T_c and Θ_D . Thus, for systems with $\lambda > 1$ the McMillan equation often failed to accurately capture the superconducting behavior.

Subsequently, Allen and Dynes published a modified version of the McMillan equation⁹³ to estimate T_c :

$$T_c = \frac{\omega_{\text{ln}}}{1.2} \exp \left[- \frac{1.04(1 + \lambda)}{\lambda - \mu^*(1 + 0.62\lambda)} \right]. \quad (5)$$

This equation was based on 217 numerical solutions of the Eliashberg equations for $0 \leq \mu^* < 0.2$, $0.3 < \lambda < 10$, and $\alpha^2 F(\omega)$ shapes of Pb and Hg obtained from the known

tunneling experiments, as well as an Einstein model, which includes no Coulombic repulsion ($\mu^*=0$) and whose shape of $\alpha^2 F(\omega)$ maximizes T_c for given values of λ and ω_{ln} .

In an earlier work, Dynes had replaced the $\frac{\Theta_D}{1.45}$ prefactor in the McMillan equation (Equation 3) with a prefactor of $\frac{\langle \omega \rangle}{1.2}$.⁹⁴ In the Allen-Dynes modified McMillan equation (Equation 5) $\langle \omega \rangle$ was further replaced with the logarithmic average phonon frequency, ω_{ln} , calculated as

$$\omega_{\text{ln}} = \exp \left[\frac{2}{\lambda} \int_0^\infty \frac{d\omega}{\omega} \alpha^2 F(\omega) \ln(\omega) \right]. \quad (6)$$

This procedure was found to drastically reduce the dependence of T_c on the shape of the spectral function, resulting in an expression that is quite accurate for predicting T_c for materials with $\lambda < 1.5$.

In a computational study, the Eliashberg spectral function can be calculated for a material using DFT codes including the Quantum Espresso⁹⁵, ABINIT⁹⁶, and EPW⁹⁷ packages from which values for λ can be obtained and T_c can be estimated via Equation 5. Typically, a range of T_c values corresponding to solutions where $0.1 \leq \mu^* \leq 0.13$ or 0.15 is given in an article. In strongly coupled systems, however, where $\lambda > 1.5$, the T_c estimated with Equation 5 is too low. In these cases, the usual course is either numerical solution of the Eliashberg equations⁹¹ to generate a more appropriate estimate of T_c , or the application of correction factors f_1 (for strong coupling) and f_2 (for shape dependence).⁹³ The approximate form for these factors is given by

$$f_1 = \left\{ 1 + \left[\frac{\lambda}{2.46(1 + 3.8\mu^*)} \right]^{\frac{3}{2}} \right\}^{\frac{1}{3}}, \quad (7)$$

and

$$f_2 = 1 + \frac{(\omega_2/\omega_{\text{ln}} - 1)\lambda^2}{\lambda^2 + [1.82(1 + 6.3\mu^8)(\omega_2/\omega_{\text{ln}})]^2} \quad (8)$$

where the logarithmic average of the phonon frequency ω_{ln} is calculated as in Equation 6 and ω_2 is

$$\omega_2 = \left[\frac{2}{\lambda} \int_0^\infty \omega \alpha^2 F(\omega) d\omega \right]^{1/2}. \quad (9)$$

An alternative way to calculate T_c is via density functional theory for superconductors (SCDFT)⁹⁸. By creating a density functional framework based on the system electron density, N-body nuclear interactions, and the superconducting order parameter⁹⁸⁻¹⁰⁰, it does not rely on empirical parameters such as the effective Coulombic repulsion term μ^* .

III. HYDROGENIC MOTIFS

A. Mixed Molecular and Atomic Hydrogen

Within these hydride phases, the hydrogen sublattice can assume many forms – atomic/hydridic hydrogen, molecular

H_2 and H_3^- (and more exotic) units, weakly covalent clathrate cages, and more. One ubiquitous group of phases are those with a mixture of atomic H and molecular H_2 . Among these, the presence of distinct hydrogenic motifs is associated with varying degrees of electron transfer to and from the molecular and atomic units, which strongly influences the electronic structure and superconducting properties of the resulting phases. An immensely common structure type among metal hydride phases is the $I4/mmm$ symmetry phase (Figure 2a) of which $ThCr_2Si_2$ and $BaAl_4$ are archetypes. In this geometry, electropositive metal atoms occupy the $2a$ Wyckoff positions and hydrogen atoms are distributed between the apical (Wyckoff position $4e$) and basal (Wyckoff position $4d$) sites. Within $ThCr_2Si_2$ the Si/Cr atoms lie on the $4e/4d$ sites.

Depending on the volume of the unit cell and amount of electron transfer between the metallic and hydrogenic lattices, the apical hydrogens, H_a , can be treated as weakly bonded to nearly hydridic in character, while the basal hydrogens, H_b , are generally formally considered hydridic, so that the overall distribution of charge can be expressed as $M^{x+}(H_b^-)_2(H_a)_2^{(x-2)-}$. This phase has been predicted to lie on the convex hull of numerous metal-hydrogen binary systems: CaH_4 ^{42,101,102}, SrH_4 ^{103,104}, ScH_4 ¹⁰⁵⁻¹⁰⁷, YH_4 ^{44,108}, LaH_4 ⁴⁴, CeH_4 ^{43,109,110}, PrH_4 ^{43,111,112}, PuH_4 ⁷⁶, EuH_4 ¹¹³, NdH_4 ^{43,114}, TbH_4 ⁷⁷, ThH_4 ^{113,115} and ZrH_4 ¹¹⁶. In addition, model convex hulls based on computed enthalpies for a series of ubiquitous structure types observed in metal hydride structures found PmH_4 , SmH_4 , EuH_4 , GdH_4 , TbH_4 , DyH_4 , HoH_4 , ErH_4 , TmH_4 , and LuH_4 to be stable⁴³.

The staggering array of binary systems for which this structure is stable lends itself well to probing property trends based on character of the metal element, as seen in a recent overview.¹¹⁷ Oxidation states for M^{x+} range from 2+ to 4+, with CaH_4 and ThH_4 as exemplars, resulting in different amounts of electron density donated to the hydrogen lattice. The added electron density weakens the H_a - H_a bonds via a two-pronged mechanism involving population of the H_2 σ_u^* antibonding orbitals as well as a Kubas-like interaction of coupled H_2 $\sigma_g \rightarrow M d$ and $M d \rightarrow H_2 \sigma_u^*$ donation. Thus, the H_a - H_a bond distance depends greatly on the valency of the metal atom, with the divalent tetrahydrides having H_a - H_a distances slightly longer but comparable to molecular H_2 , while the tetravalent hydrides have H_a - H_a distances nearly twice as long (with four electrons per formula unit donated to the hydrogen lattice, each hydrogen will have a formal charge of -1, corresponding to hydridic character). Hoffmann and Zheng have shown that the X-X bond in the AB_2X_2 structure type can be tuned by the choice of the transition metal atom^{118,119}, similar to what we find here for the H_a - H_a contact.

The distance dependence of the H_a - H_a contact on the valence and size of the metal atom has noteworthy consequences on the predicted T_c s, whose values are recorded in Table I. In MgH_4 , which has an estimated T_c of 126 K at 300 GPa¹¹⁷, a major contributor to the EPC constant λ involved libration of the H_a - H_a units coupled to interactions with the H_b network. One phonon mode with an especially large EPC contribution involved circular motions of the H_b atoms which, upon decreasing pressure, softens to the point of instability. Often, su-

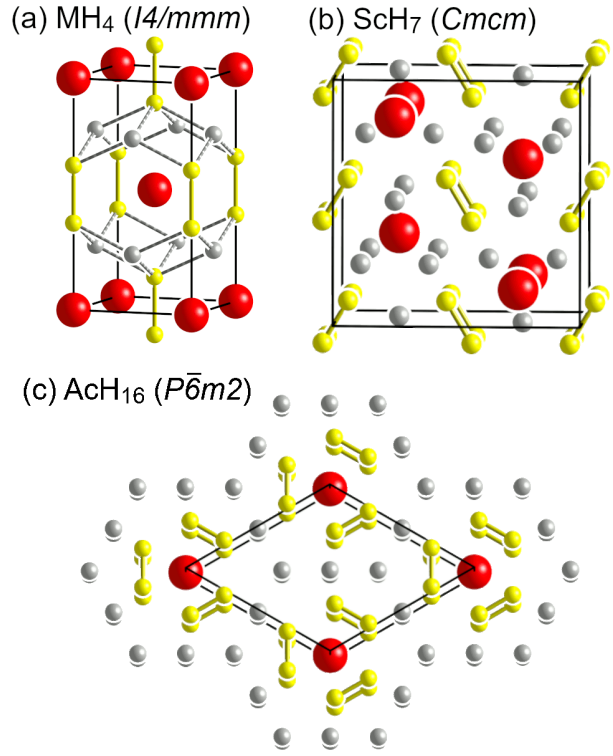


FIG. 2. Structures of metal hydride phases with atomic H and molecular H_2 units with metal atoms in red, atomic H in grey, and molecular H_2 units in yellow. (a) $I4/mmm$ structure common to several MH_4 phases has apical hydrogens, H_a , in molecular units and atomic basal hydrogens, H_b . (b) ScH_7 structure ($Cmcm$) with alternating layers of H_2 units and atomic H with Sc. (c) $P6m2$ AcH_{16} structure with three H_2 units above and below each Ac, which is also coordinated to 12 atomic H.

perconductivity is favored near the onset of dynamic instability. In YH_4 , where the metal is formally trivalent, strong contributions to the EPC arise along a soft phonon mode around the N point that is related to the motions of the H_a atoms¹⁰⁸. Large contributions to the EPC within ScH_4 arise mostly from motions of the H_a atoms, one of which involves a similar coupling of a H_a - H_a libration to the H_b network as in MgH_4 ¹¹⁷.

Lower T_c s are associated with LaH_4 ⁴⁴, ZrH_4 ¹¹⁶, and ThH_4 ¹¹⁵. Even though La is a trivalent metal like Sc and Y whose $I4/mmm$ MH_4 structures exhibit moderate to high T_c s, the T_c of LaH_4 is predicted to be an order of magnitude smaller. Two explanations have been provided. First, La has a higher mass than its trivalent congeners, which is associated with reductions in phonon-mediated T_c ⁴⁴. Another facet is related to the increase in H_a - H_a distance – and decrease in interaction strength as shown by the calculated crystal orbital Hamilton populations integrated to the Fermi level (-iCOHP) values between the H_a atoms – owing to La's large size¹¹⁷. The low estimated T_c in ThH_4 arises from a similar lack of H_a - H_a interaction¹¹⁵. On the other hand, the H_a - H_a distance in ZrH_4 is more in line with that in trivalent metal tetrahydrides (Zr would be expected to be tetravalent), and its lower T_c is likely due to the increased mass of Zr decreasing the

TABLE I. Superconducting properties of select binary hydrides with mixed molecular and atomic hydrogen (Figure 2).

Structure (space group)	Pressure (GPa)	λ	μ^*	T_c
ScH ₄ ¹¹⁷ (<i>I4/mmm</i>)	120	1.19	0.13-0.1	113.3-101.5 ^a , 92.3-81.8 ^b
ScH ₄ ¹⁰⁷ (<i>I4/mmm</i>)	120	1.68	0.1	163 ^a , 92 ^b
ScH ₄ ¹⁰⁵ (<i>I4/mmm</i>)	195	0.89	0.13-0.1	67-81 ^b
ScH ₄ ¹⁰⁶ (<i>I4/mmm</i>)	200	0.99	0.1	98 ^b
ZrH ₄ ¹¹⁷ (<i>I4/mmm</i>)	150	1.24	0.13-0.1	77.1-66.1 ^a , 58.9-52.4 ^b
ZrH ₄ ¹¹⁶ (<i>I4/mmm</i>)	230	0.89	0.19	47 ^a
MgH ₄ ¹¹⁷ (<i>I4/mmm</i>)	255	1.05	0.13-0.1	124.7-105.0 ^a , 112.9-98.4 ^b
MgH ₄ ¹¹⁶ (<i>I4/mmm</i>)	255	0.88	0.13	81 ^a
MgH ₄ ¹²⁰ (<i>I4/mmm</i>)	100	0.74	0.13-0.1	29-37 ^b
YH ₄ ¹⁰⁸ (<i>I4/mmm</i>)	120	1.01	0.13-0.1	84-95 ^a
TbH ₄ ⁷⁷ (<i>I4/mmm</i>)	200	0.70	0.13-0.1	31.3-41.3 ^b
LaH ₄ ⁴⁴ (<i>I4/mmm</i>)	300	0.43	0.13-0.1	5-10 ^a , 5-10 ^b
ScH ₇ ¹⁰⁷ (<i>Cmcm</i>)	300	1.84	0.1	213 ^a , 169 ^b
AcH ₁₆ ¹²¹ (<i>P6̄m2</i>)	150	2.16	0.15-0.1	221-241 ^a , 171.3-199.2 ^b

^a T_c was calculated using the Allen-Dynes modified McMillan equation (Equation 5)

^b T_c was calculated by numerical solution of the Eliashberg equations

value of ω_{in} ¹¹⁶. In contrast to what is found for MgH₄, CaH₄ and SrH₄ develop only a small DOS at E_F from pressure induced band overlap, and are therefore unlikely to be good superconductors.

Due to its ubiquity, we have thus far focused on the *I4/mmm* ThCr₂Si₂ structure, whose proclivity towards superconductivity varies greatly based on the metallic element. Metal atoms need to donate sufficient electron density to weaken H_a-H_a interactions – but not too much, and they need to be large enough to stretch the H_a-H_a distance - but not too much. Fully breaking covalent interactions results in an essentially hydridic lattice, while weakening them with partial occupancy of H₂ σ^* bands results in a metallic lattice with sizable DOS at E_F , as in YH₄. Conversely, phases with very low electron transfer into the H₂ units, as in CaH₄, undergo metallization through pressure-induced broadening of H⁻ and H₂ σ^* bands. This situation, fairly common in metal hydride phases mixing molecular H₂ units with atomic H, tends to result in a low projected H DOS at E_F and poor propensity towards superconductivity.

In addition to *I4/mmm* ScH₄, the Sc-H system contains another phase mixing atomic and molecular H₂ – *Cmcm* ScH₇. In this structure, where layers of H₂ units alternate with layers of Sc and atomic H (Figure 2b), Sc donates electron density into the molecular H₂ σ^* bands, as well as to the atomic H, stretching the H₂ distance to roughly to 0.96 Å at 300 GPa. This results in a robust DOS at E_F and, at 300 GPa, an estimated T_c of 169 K¹⁰⁷. In the Ac-H system, the *P6̄m2* AcH₁₆ structure (Figure 2c) has Ac coordinated by 12 atomic hydrogens and six H₂ units¹²¹, resulting in a moderate H-based DOS at E_F . Several other Ac-H binary phases also contain a mixture of atomic and molecular H, but they are nonmetallic. At 150 GPa, the T_c of *P6̄m2* AcH₁₆ is estimated to be 241 K with a large $\lambda=2.16$, although a strong pressure dependence is expected as a result of its layered structure.

B. Clathrate based hydrogenic lattices

A calcium hydride compound consisting of Ca embedded in a curious “sodalite-like” hydrogenic cage⁴², shown in Figure 3a, was the first in a long series of predicted phases featuring clathrate-like hydrogenic cages and remarkably high T_c s (Table II). In a great success for theory, the predictions for a number of members belonging to this class of structures have since been experimentally verified^{3-7,122}. In 2012, the aforementioned CaH₆ phase was predicted to be stable above 150 GPa in a crystal structure with *Im3̄m* symmetry⁴² soon found to be shared by several other high pressure MH₆ compounds, including MgH₆¹²³, YH₆^{43,108}, ScH₆^{43,106,107}, PuH₆⁷⁶, TbH₆⁷⁷, EuH₆⁷⁵, and (Nd-Lu)H₆^{43,124}.

This body-centered cubic structure features Ca atoms surrounded by a sodalite-like H₂₄ framework comprised of six square and eight hexagonal faces, denoted as [4⁶6⁸], with a square H₄ unit on each face of the conventional unit cell. At 150 GPa, the calculated H-H distances in CaH₆ measure 1.24 Å, shorter than the H_b-H_b distances (1.95 Å) but longer than the H_a-H_a distances (0.82 Å) in *I4/mmm* CaH₄ at the same pressure, suggestive of a weakly bound clathrate cage. The calculated electron localization function (ELF) provides further evidence for this weak bond between the H atoms, but no covalent bonds were present between Ca and H. In fact, the molecular orbital diagram predicted for a H₄ square unit possesses a half-occupied degenerate non-bonding state above the lowest-energy bonding state. If each Ca atom donated both its valence electrons to the hydrogen sublattice, each H could then possess up to 1/3 of an electron in excess, placed into this non-bonding state without having to populate an antibonding orbital. With the degenerate non-bonding state partially filled, Jahn-Teller distortions reducing the structural symmetry can lift this degeneracy, and phonon modes based on such symmetry reductions can contribute strongly to superconductivity by way of the EPC parameter. The calculated EPC of CaH₆ is remarkably large, $\lambda=2.69$ and $T_c=220-235$ K at 150 GPa,

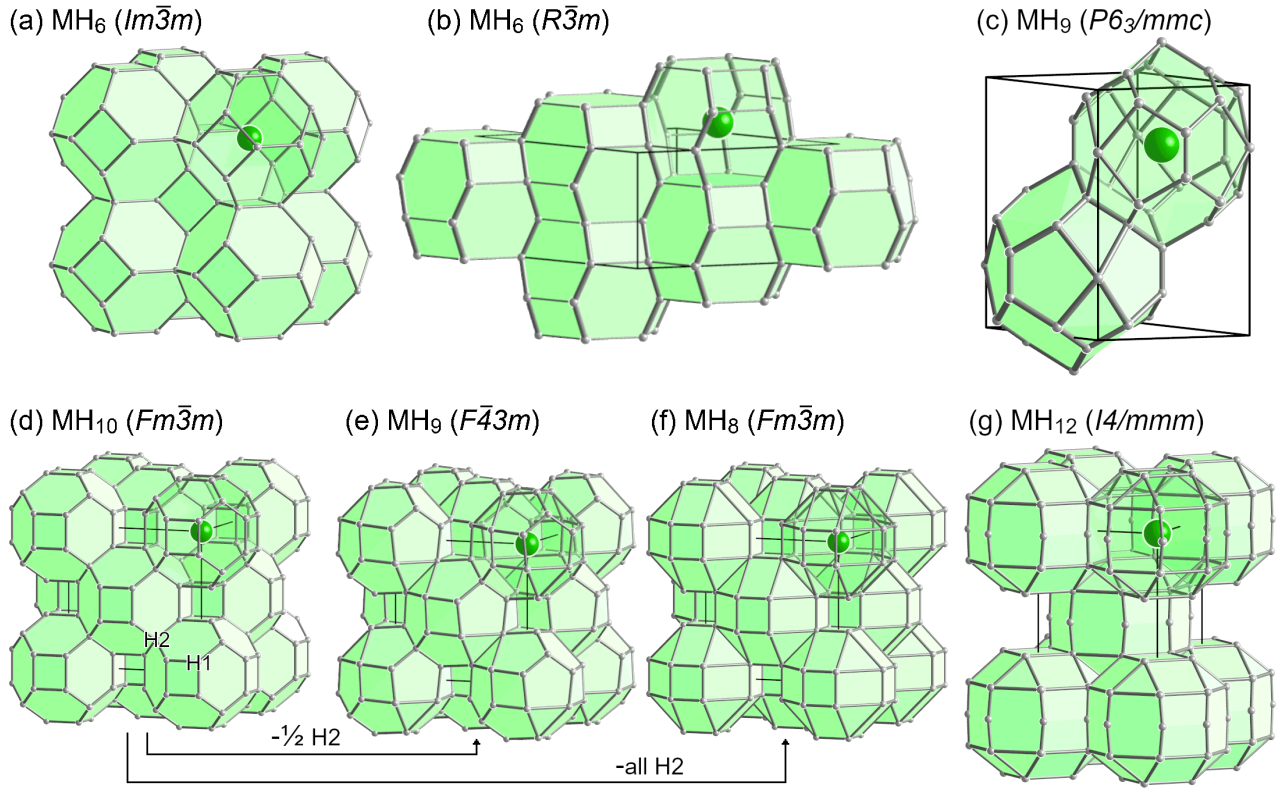


FIG. 3. Metal hydride structures with clathrate-like hydrogenic lattices. (a) $Im\bar{3}m$ symmetry structure adopted by several MH_6 phases with a body-centered lattice of $M@H_{24}$ polyhedra. (b) Distorted $M@H_{24}$ polyhedra comprising an $R\bar{3}m$ phase adopted by some MH_6 compounds with larger metal atoms. (c) $P6_3/mmc$ structure adopted by several MH_9 phases based on $M@H_{29}$ polyhedra. (d) $Fm\bar{3}m$ structure adopted by several MH_{10} phases based on $M@H_{32}$ polyhedra with H1 (32f) and H2 (8c) sites. Removing half of the H2 atoms generates the (e) $F\bar{4}3m$ phase adopted by some MH_9 compounds, while removing all H2 atoms from the $Fm\bar{3}m$ MH_{10} lattice yields (f) the $Fm\bar{3}m$ structure adopted by some MH_8 compounds. (g) $I4/mmm$ structure adopted by AcH_{12} with similar coordination polyhedra to the $Fm\bar{3}m$ MH_8 structure where additional H atoms bisect eight of the square faces.

with most of the EPC being derived from symmetry breaking breathing and rocking motions within the H_4 units at Γ as favored by the Jahn-Teller effect.

This discovery prompted numerous investigations into the possibility that other metal hydrides could possess similar structures when squeezed. In short order, a YH_6 phase isotopic to CaH_6 was predicted to be stable above 110 GPa when including ZPE effects¹⁰⁸. With a calculated $\lambda=2.93$ at 120 GPa, the T_c was estimated to be 251-264 K, even higher than the prediction for CaH_6 . The shape of the Eliashberg spectral function was quite different from CaH_6 ; while the EPC in CaH_6 was found mostly to arise from T_{2g} and E_g modes at the Γ point, the contributions to the EPC in YH_6 were much more dispersed throughout the phonon band structure. YH_6 has been synthesized at 160 GPa, where its T_c was measured to be 224 K⁷, lower than the initial theory predictions. The inclusion of anharmonic effects and setting $\mu^*=0.19-0.22$ were needed for the calculated T_c to match up with experiment.

It did not take long before theory predicted that MgH_6 ¹²³ and ScH_6 ^{43,106,107} $Im\bar{3}m$ phases would be stable above 263 GPa and 275 GPa, respectively. Similar to YH_6 , the

contributions to the EPC in MgH_6 were spread throughout the Brillouin zone. Several polymorphs of ScH_6 have been predicted, with symmetries including $Cmcm$ ¹⁰⁷ and $P6_3/mmc$ ^{43,106,107}, suggesting complex phase behavior under pressure. Finally, recent explorations of the rare earth hydrides have identified Pu ⁷⁶, Tb ⁷⁷, Eu ⁷⁵, and $Pm-Lu$ ¹²⁴ analogues, with TbH_6 having an estimated T_c up to 147 K at 300 GPa.

In addition to these, a number of other high-pressure MH_6 phases have been predicted with crystal structures that can be derived from distortions of the highly symmetric H_{24} polyhedra that comprise the $Im\bar{3}m$ structure. One example is ZrH_6 , which forms a phase with $I4/mmm$ symmetry above 275 GPa¹¹⁶, although it is very close in energy to a $P2_1/c$ structure until 320 GPa. This $I4/mmm$ structure is obtained by slightly stretching the cubic $Im\bar{3}m$ phase to a c/a ratio of 1.08. More complex distortions occur in the $R\bar{3}m$ structure predicted for SrH_6 , in which opposite hexagonal faces in the sodalite-like H_{24} framework are opened up, resulting in a helical hydrogenic arrangement^{103,104} (Figure 3b). Imaginary phonon modes calculated at low pressures involve the formation of $H_2 \cdots H^-$ configurations along the helical chains

and indicate possible liquid-like behavior as has been proposed in other hydride phases^{125,126}. SrH₆ is a good metal, owing to equidistant 1-dimensional arrangements of H atoms with some electron donation from Sr, analogous to the electron transfer from Ca to H in CaH₆, resulting in a calculated T_c of 156 K at 250 GPa³⁵. LaH₆ has also been predicted to form in this structure type at pressures of \sim 100-150 GPa^{43,44}, although not necessarily to lie on the La-H convex hull. The H₂₄ cage is further broken up in an *Imm2* structure predicted for BaH₆, in which H₃⁻ units are present¹²⁷. Several possible BaH₆ geometries are nearly isoenthalpic over a range of pressures, with various hydridic, molecular, or H₃⁻ motifs present in each.

Hydrogenic clathrate-like cages are also prevalent for the MH₉ stoichiometry. The predicted structure with the highest symmetry is a *P6₃/mmc* arrangement of M@H₂₉ cages with a [4⁶5⁶6⁶] framework (Figure 3c), and H-H distances slightly elongated relative to molecular H₂. Several phases have been predicted to assume this structure, including YH₉^{43,44}, ScH₉⁴³, CeH₉^{110,124}, LaH₉⁴³, NdH₉^{114,124}, and (Pr-Er)H₉¹²⁴. *P6₃/mmc* PrH₉¹¹⁴ and EuH₉⁷⁵ have been identified in experiments, although in both cases a different structure was calculated to lie on the convex hull – an *F43m* geometry for PrH₉^{112,124} and a *P1* Eu₄H₃₆ phases that arises from small distortions⁷⁵.

P6₃/mmc YH₉ (which lies on the convex hull above 200 GPa^{43,44}) has a remarkably large EPC constant, $\lambda=4.42$ at 150 GPa⁴³. A synthesized yttrium superhydride with a measured T_c of 262 K at ca. 180 GPa has been assigned as *P6₃/mmc* YH₉⁵ on the basis of Raman spectroscopy, although a second experimental study found its T_c to be roughly 20 K lower: 243 K at 201 GPa⁶. CeH₉ has an estimated T_c of 74-87 K at 250 GPa¹²⁴ and 105-117 K at 200 GPa¹¹⁰ but has also been experimentally observed at much lower pressures^{110,132,133}, where its T_c was measured to be 57 K at 88 GPa increasing to 100 K at 130 GPa¹³³. Its shortest H-H distances at 100 GPa were 1.116 Å, much shorter than in LaH₁₀, and in fact approaching the interatomic distances in atomic H¹¹⁰. The markedly low pressure of 80 GPa at which CeH₉ was detected has been proposed to arise from particularly strong chemical precompression levied by the delocalized *4f* electrons of Ce, suggesting that other rare earth hydrides with similar delocalized *f* character may also be stabilized at relatively low pressures¹³⁴. The low measured T_c for (metastable) *P6₃/mmc* PrH₉, < 9 K at 120 GPa¹¹⁴, was ascribed to the very small ($<10\%$) contribution from H states to the DOS at E_F , which was mostly comprised of Pr *f* character. In fact, theoretical calculations suggest that many of the lanthanide MH₉ polyhydrides have a DOS at E_F dominated by the M *f* states, resulting in estimated T_c values < 10 K¹²⁴.

As in the case of the MH₆ stoichiometry, MH₉ phases with structures based on distortions of the M@H₂₉ clusters have also been proposed. One example is a *C2/m* symmetry CaH₉ structure stable above 235 GPa¹⁰². H₂ and bent H₃ motifs comprise its hydrogenic network, reducing the overall symmetry of the H₂₉ cluster. Compared to *P6₃/mmc* YH₉, in which three valence electrons are available for donation into the hydrogen network, Ca can only donate two, reflected in the

calculated Bader charges. With fewer donated electrons occupying nonbonding or antibonding orbitals in the hydrogenic framework, the H₂ and H₃ units in *C2/m* CaH₉ remain intact rather than disproportionating into the H₂₉ cluster present in YH₉ where the H-H contacts are nearly equidistant. Finally, a TbH₉ phase with *C2/c* symmetry was predicted to be stable above 175 GPa⁷⁷, although another study found only the *P6₃/mmc* structure above 250 GPa¹²⁴.

Among the most promising candidates for high temperature superconductivity identified by CSP techniques are the LaH₁₀ and YH₁₀ phases, for which an *Fm3m* structure is predicted^{43,44,124}. The hydrogenic network in this symmetry contains H₃₂ clusters with a [4⁶6¹²] framework (shown in Figure 3d). Another way to view these structures are as metal atoms and H₈ hydrogen cubes comprising an interlocking fcc pattern. Hydrogen atoms occupy the 32*f* (H1) and 8*c* (H2) Wyckoff positions in the structure, with the H1 atoms forming square faces on the H₃₂ polyhedron, and the H2 atoms lying at the center of an (H1)₄ tetrahedron. The predicted T_c values for LaH₁₀ and YH₁₀ were among the highest obtained for the metal clathrate superhydrides, 257-274 K for LaH₁₀ at 250 GPa⁴⁴, and 305-326 K for YH₁₀ at 250 GPa⁴⁴. Although the EPC constant is lower for YH₁₀ than YH₆ (2.56 vs. 2.93), the higher hydrogen content in YH₁₀ leads to a larger average phonon frequency, ω_{ln} , and thus a very large expected T_c ⁴⁴. Because room temperature superconductivity is predicted in YH₁₀ its synthesis has been attempted, but so far only YH₆ and YH₉ have been made⁵⁻⁷. LaH₁₀ has successfully been synthesized¹³⁵, with a measured T_c of 250 K at 170 GPa⁴ and 260 K at 185 GPa³.

Several additional REH₁₀ phases assuming *Fm3m* symmetry have been predicted, including CeH₁₀^{43,109,124}, which has a maximum estimated T_c of 156-168 K at 94 GPa¹⁰⁹ (although some studies also propose an *R3m* phase with a much lower estimated T_c of < 56 K⁴³). *Fm3m* CeH₁₀ has been observed experimentally with a measured T_c of 115 K at 95 GPa¹³³. Alongside CeH₉, this reflects the impressive ability of cerium hydrides to maintain stability to – for high- T_c metal hydrides – remarkably low pressures. PrH₁₀^{43,124}, PuH₁₀⁷⁶, UH₁₀¹³⁶, and (Nd-Dy, Yb)H₁₀¹²⁴ *Fm3m* phases have all been proposed to lie on the convex hull at various elevated pressures, and UH₁₀ has an estimated T_c of 7-15 K at 550 GPa¹³⁶. An *Fm3m* phase is proposed to be near-isoenthalpic with an *R3m* structure for TbH₁₀; with estimated T_c s roughly 270 K above 230 GPa and 270 GPa for the *Fm3m* and *R3m* structures, respectively⁷⁷.

Analogous to what is found for certain MH₆ and MH₉ phases, the *R3m* MH₁₀ structure can be derived by a distortion of the parent clathrate *Fm3m* phase where the hydrogenic network is broken up into puckered graphene-like nets. For the Ac-H¹²¹ and Sr-H¹⁰⁴ systems the *R3m* configuration is predicted to be preferred, for which AcH₁₀ has an estimated T_c of 226-251 K at 200 GPa¹²¹. In contrast to CeH₁₀ and TbH₁₀, which have been predicted to assume both structure types, so far calculations have only located *R3m* CaH₁₀, which lies slightly above the convex hull at 400 GPa, with an estimated T_c of 157-175 K¹⁰².

These complex structural relationships encourage careful

TABLE II. Superconducting properties of select binary metal hydrides with clathrate-like hydrogen cages (Figure 3).

Structure (space group)	Pressure (GPa)	λ	μ^*	T_c (K)
MgH ₆ ¹²³ (<i>Im</i> $\bar{3}m$)	300	3.29	0.12	263 ^a
CaH ₆ ⁴² (<i>Im</i> $\bar{3}m$)	150	2.69	0.13-0.1	220-235 ^b
ScH ₆ ⁴³ (<i>Im</i> $\bar{3}m$)	300	1.2 ^c	0.13-0.1	90-100 ^{b,c}
ScH ₆ ¹⁰⁵ (<i>Im</i> $\bar{3}m$)	285	1.33	0.13-0.1	130-147 ^a
ScH ₆ ¹⁰⁷ (<i>Im</i> $\bar{3}m$)	350	1.25	0.1	135 ^a , 169 ^b
YH ₆ ¹⁰⁸ (<i>Im</i> $\bar{3}m$)	120	2.93	0.13-0.1	251-264 ^b
YH ₆ ⁴³ (<i>Im</i> $\bar{3}m$)	120	2.9 ^c	0.13-0.1	250-260 ^{b,c}
YH ₆ ¹²⁸ (<i>Im</i> $\bar{3}m$)	300	1.73	0.11	290 ^d
SrH ₆ ³⁵ (<i>R</i> $\bar{3}m$)	250	1.10	0.1	108 ^a , 156 ^b
LaH ₆ ⁴³ (<i>R</i> $\bar{3}m$)	100	1.9 ^c	0.13-0.1	155-165 ^{b,c}
LaH ₆ ¹²¹ (<i>Im</i> $\bar{3}m$) ^e	180	2.41	0.15-0.1	180-207 ^a , 217-235 ^b
TbH ₆ ⁷⁷ (<i>Im</i> $\bar{3}m$)	200	1.58	0.13-0.1	132.6-148.3 ^a
ZrH ₆ ¹¹⁶ (<i>I4/mmm</i>)	295	1.20	0.13	114 ^b
PaH ₈ ¹²⁹ (<i>Fm</i> $\bar{3}m$) ^e	10	1.58	0.13-0.1	71.4-79.4 ^{a,e}
LuH ₈ ¹²⁴ (<i>Immm</i>)	300	2.18	0.13-0.1	80.9-86.2 ^a
LaH ₈ ⁴⁴ (<i>C2/m</i>)	300	1.12	0.13-0.1	114-131 ^a
AcH ₈ ¹²¹ (<i>C2/m</i>)	150	1.79	0.15-0.1	114.1-134 ^a , 134-149 ^b
ScH ₉ ⁴³ (<i>P6₃/mmc</i>)	400	1.3 ^c	0.13-0.1	170-180 ^{b,c}
YH ₉ ⁴³ (<i>P6₃/mmc</i>)	150	4.42	0.13-0.1	253-276 ^b
LaH ₉ ⁴³ (<i>P6₃/mmc</i>)	50	0.6 ^c	0.13-0.1	20-30 ^{b,c}
CeH ₉ ⁴³ (<i>P6₃/mmc</i>)	100	0.5 ^c	0.13-0.1	40-50 ^{b,c}
CeH ₉ ¹²⁴ (<i>P6₃/mmc</i>)	250	0.97	0.13-0.1	86.8-74.1 ^a
CeH ₉ ¹¹⁰ (<i>P6₃/mmc</i>)	200	2.30	0.15-0.1	105-117 ^a
YbH ₉ ¹²⁴ (<i>P6₃/mmc</i>)	250	1.02	0.13-0.1	68.5-79.6 ^a
CaH ₉ ¹⁰² (<i>C2/m</i>)	400	2.27	0.13-0.1	206.1-219.2 ^a , 260.6-285.2 ^f
YH ₁₀ ⁴⁴ (<i>Fm</i> $\bar{3}m$)	250	2.56	0.13-0.1	305-326 ^b
YH ₁₀ ⁴³ (<i>Fm</i> $\bar{3}m$)	400	2.41	0.13-0.1	287-303 ^b
YH ₁₀ ¹²⁸ (<i>Fm</i> $\bar{3}m$)	300	2.41	0.11	310 ^d
LaH ₁₀ ⁴⁴ (<i>Fm</i> $\bar{3}m$)	250	2.2	0.13-0.1	257-274 ^b
LaH ₁₀ ¹³⁰ (<i>C2/m</i>)	200	3.57	0.13-0.1	229-245 ^a
LaH ₁₀ ¹²⁴ (<i>Fm</i> $\bar{3}m$)	250	2.25	0.13-0.1	210.4-223.9 ^a
CeH ₁₀ ⁴³ (<i>Fm</i> $\bar{3}m$)	200	0.5 ^c	0.13-0.1	50-60 ^{b,c}
CeH ₁₀ ¹²⁴ (<i>Fm</i> $\bar{3}m$)	250	0.59	0.13-0.1	43.8-30.6 ^a
YbH ₁₀ ¹²⁴ (<i>Fm</i> $\bar{3}m$)	250	1.10	0.13-0.1	89.2-102.1 ^a
TbH ₁₀ ⁷⁷ (<i>Fm</i> $\bar{3}m$)	270	2.25	0.13-0.1	247.9-272.7 ^{a,e}
TbH ₁₀ ⁷⁷ (<i>R</i> $\bar{3}m$)	270	2.86	0.13-0.1	191.8-212.5 ^a
AcH ₁₀ ¹²¹ (<i>R</i> $\bar{3}m$)	200	3.46	0.15-0.1	177-204.1 ^a , 226-251 ^b
CaH ₁₀ ¹⁰² (<i>R</i> $\bar{3}m$)	400	1.67	0.13-0.1	137.9-146.5 ^a , 156.9-175.3 ^{e,f}
AcH ₁₂ ¹²¹ (<i>I4/mmm</i>)	150	1.42	0.15-0.1	103.7-123.3 ^a , 148-173 ^b

^a T_c was calculated using the Allen-Dynes modified McMillan equation (Equation 5)

^b T_c was calculated by numerical solution of the Eliashberg equations

^c Values estimated from Figure 4 in Ref. 43

^d Values calculated using fully anisotropic Migdal-Eliashberg theory as implemented in EPW^{97,131}

^e Metastable at this pressure

^f T_c was calculated using the Allen-Dynes modified McMillan equation with strong coupling and shape corrections (Equations 7 and 8)

treatment of the energetics of competing phases, and the consideration of effects that go beyond the static lattice approximation. In the first reported synthetic study of LaH₁₀, an fcc lattice corresponding to the *Fm* $\bar{3}m$ structure was detected but then, with decompression, was observed to undergo a rhombohedral distortion¹³⁵ to *C2/m* symmetry (itself a distortion of the aforementioned *R* $\bar{3}m$ structure, with the La atoms maintaining *R* $\bar{3}m$ symmetry themselves). The estimated T_c of this distorted phase was 229-245 K¹³⁰, a formidable albeit lower value than the predicted T_c for the cubic phase (257-

274 K⁴⁴). Further theoretical work showed that the inclusion of quantum anharmonic effects had the dual effect of stabilizing the *Fm* $\bar{3}m$ phase over the competing less symmetric variants as well as extending the predicted pressure stability range for the *Fm* $\bar{3}m$ symmetry⁸⁰. It may be that these effects are also important in smoothing out the PES of the previously discussed MH₆, MH₉ and MH₁₀ stoichiometry phases that are distortions of the high-symmetry clathrates. Moreover, such quantum and anharmonic effects have been shown to suppress superconductivity in AlH₃⁸¹, while quantum nuclear effects

stabilize $Im\bar{3}m$ symmetry in the high- T_c H_3S compound¹³⁷, highlighting their potential importance for the properties of metal hydrides.

Another family of structural derivatives of $Fm\bar{3}m$ MH_{10} is generated by removing some or all of the $8c$ H2 atoms leading to either an $F\bar{4}3m$ symmetry MH_9 (if half of the H2 atoms are removed, Figure 3e), or an $Fm\bar{3}m$ symmetry MH_8 (if all of the H2 atoms are removed, Figure 3f) stoichiometry. Two examples of the former are the cubic CeH_9 ¹¹⁰ and PrH_9 ^{112,124} phases expected to form instead of the $P6_3/mmc$ structure that was experimentally observed^{110,112,114}. $F\bar{4}3m$ PaH_9 ¹²⁹ and $(Pr-Sm, Ho, Yb)H_9$ ¹²⁴ phases have also been predicted. Examples of the latter include predicted $Fm\bar{3}m$ phases for $(Nd, Ho-Tm)H_8$ ¹²⁴, PaH_8 ¹²⁹, PuH_8 ⁷⁶, and UH_8 ^{136,138}, while LuH_8 ¹²⁴ is expected to form in an $Immm$ tetragonally distorted version of the structure. At 300 GPa, LuH_8 has an estimated T_c of 81-86 K¹²⁴, while PaH_8 reaches the convex hull at the remarkably low pressure of 32 GPa and maintains dynamic stability below 10 GPa, where its estimated T_c is 71-79 K¹²⁹. An additional $F\bar{4}3m$ PaH_5 stoichiometry is an even more extreme modification: every other $H2@(H1)_4$ tetrahedron of the $Fm\bar{3}m$ MH_{10} structure is fully removed¹²⁹.

LaH_8 ⁴⁴, AcH_8 ¹²¹, and YH_8 ⁴⁴ phases have also been predicted, although with $C2/m$ symmetry for La and Ac and Cc symmetry for Y. Fragments of the $Fm\bar{3}m$ MH_{10} and $Im\bar{3}m$ MH_6 geometries appear in LaH_8 and AcH_8 . For even higher H content, an AcH_{12} phase with $I4/mmm$ symmetry is metastable (by 0.05-0.06 eV/atom) in the 150-300 GPa pressure range¹²¹. Each Ac atom lies within a distorted rhombicuboctahedron of H atoms wherein one of the square faces has two additional H atoms along opposite edges (Figure 3g). A metastable RbH_{12} phase with $Immm$ symmetry was found close to the convex hull at the impressively low pressure of 50 GPa, where it has an estimated T_c of 115 K, increasing slightly to 126 K at 150 GPa³⁷. High-frequency phonon modes involving motions of the hydrogen cage contributed strongly to the overall EPC of this structure. Notably, this study employed machine learning models to suggest high T_c superconductors that were stable at lower pressures, illustrating the utility of machine learning methods in choosing promising systems.

C. Other geometrical motifs

Most high- T_c superconducting hydrides can be classified as possessing hydrogen lattices involving mixed atomic and molecular hydrogen (MgH_4), clathrate-like structures (LaH_{10}), or covalent 3D networks (H_3S), in which the electronic structure of the system is responsive to H atom motions, thereby conferring a strong EPC. Some phases, however, defy these classifications and feature curious hydrogenic motifs as well as superior superconducting properties (see Table III). The family of scandium hydrides has been found to contain several of these strange hydrogen motifs alongside the clathrate-like ScH_6 and the $ThCr_2Si_2$ -like ScH_4 . Around 300 GPa, a ScH_9 phase with $I4_1md$ symmetry¹⁰⁷ was found to be slightly lower in enthalpy than the previously predicted

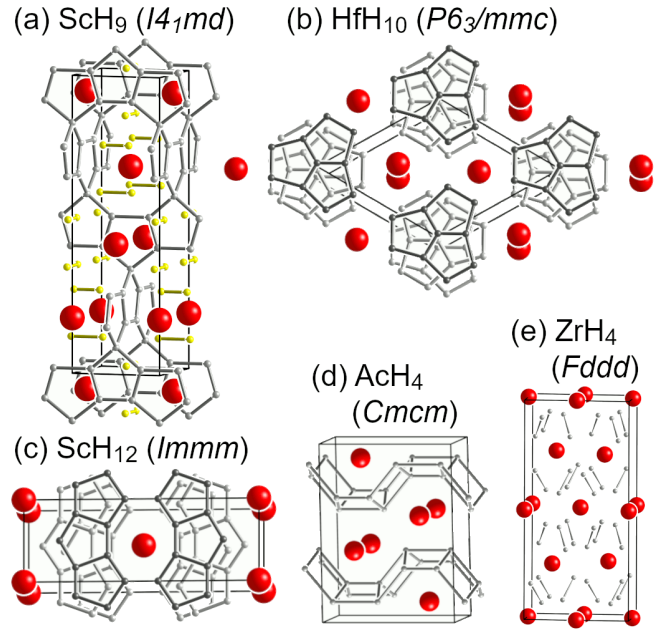


FIG. 4. Binary metal hydride structures featuring curious geometrical motifs. (a) Vertex-sharing perpendicularly oriented 1D chains of H_5 pentagons alongside molecular H_2 units in $I4_1md$ ScH_9 . (b) Stacked triads of fused H_5 pentagons in $P6_3/mmc$ HfH_{10} . (c) 1D chains of H_5 pentagons in $Immm$ ScH_{12} . (d) Buckled nets of distorted squares in $Cmcm$ AcH_4 . (e) Atomistic hydrogen in $Fddd$ ZrH_4 (shortest H-H contacts at a distance of 1.38 Å are drawn to guide the eye).

$P6_3/mmc$ symmetry clathrate⁴³. In $I4_1md$ ScH_9 , stacks of H_5 pentagons interspersed with H_2 molecular units are arranged along the a and b axes (Figure 4a). ELF plots clearly show bonding within the H_5 and H_2 units, and a fairly large EPC constant, $\lambda = 1.94$, gives rise to an estimated T_c of up to 233 K at 300 GPa.

Above 220 GPa, $Immm$ ScH_{10} is predicted to become stable¹⁰⁷. Similar to ScH_9 , this structure features H_5 pentagons, but here they are fused together in sets of three, with one pentagon fully closed and the other two slightly opened. Layers of the fused pentagons – where bonding interactions are again revealed via plots of the ELF – alternate with layers of Sc atoms. Essentially isoenthalpic with this structure is another ScH_{10} geometry^{41,43} – also based on triads of fused H_5 pentagons, but this time with $P6_3/mmc$ symmetry (Figure 4b). In this structure, the fused “pentagraphene-like” units are stacked along the c axis and rotated relative to one another by 60° . It is predicted to lie only $\sim 1 - 2$ meV/atom above the convex hull as HfH_{10} , ~ 18 meV/atom above the convex hull as ZrH_{10} , and on the 300 GPa convex hull as LuH_{10} ⁴¹. Magnesium and thorium analogues – chosen for their comparable electronegativities and atomic radii to Hf and Zr – were found to be dynamically unstable, suggested to be due to insufficient electron transfer from Mg (which lacks d electrons) and the too-large size of thorium. The high T_c values estimated for (Sc, Hf, Zr, Lu) H_{10} (up to 213-234 K at 250 GPa

TABLE III. Superconducting properties of select binary metal hydrides with unique hydrogenic motifs (Figure 4).

Structure (space group)	Pressure (GPa)	λ	μ^*	T_c (K)
ScH ₉ ¹⁰⁷ (<i>I4₁md</i>)	300	1.23	0.1	163 ^a , 233 ^b
ScH ₁₀ ¹⁰⁷ (<i>Cmcm</i>)	250	1.17	0.1	120 ^a , 143 ^b
ScH ₁₀ ⁴¹ (<i>P6₃/mmc</i>)	250	1.16	0.13-0.1	99-114 ^{a,d} , 112-124 ^{b,e} , 134-158 ^f
HfH ₁₀ ⁴¹ (<i>P6₃/mmc</i>) ^c	250	2.77	0.13-0.1	152-167 ^{a,d} , 226-239 ^{b,e} , 213-234 ^f
LuH ₁₀ ⁴¹ (<i>P6₃/mmc</i>)	200	1.36	0.13-0.1	105-118 ^{a,d} , 123-134 ^{b,e} , 134-152 ^f
ZrH ₁₀ ⁴¹ (<i>P6₃/mmc</i>) ^c	250	1.77	0.13-0.1	151-167 ^{a,d} , 185-198 ^{b,e} , 199-220 ^f
ScH ₁₂ ¹⁰⁷ (<i>Immm</i>)	350	1.23	0.1	141 ^a , 194 ^b
AcH ₄ ¹²¹ (<i>Cmcm</i>)	100	0.89	0.15-0.1	43.2-60 ^a , 50-67 ^b
ZrH ₄ ¹¹⁶ (<i>Fddd</i>)	140	1.08	0.13	78 ^b
ZrH ₆ ¹¹⁶ (<i>Cmc2₁</i>)	215	0.92	0.13	70 ^b
ZrH ₆ ¹¹⁶ (<i>P2₁/c</i>)	295	1.68	0.13	153 ^b

^a T_c was calculated using the Allen-Dynes modified McMillan equation (Equation 5)

^b T_c was calculated by numerical solution of the Eliashberg equations

^c Metastable at this pressure

^d T_c was calculated using the Allen-Dynes modified McMillan equation with strong coupling and shape corrections (Equations 7 and 8)

^e Matsubara-type linearized Eliashberg equations

^f Gor'kov-Kresin formalism with λ_{opt} and λ_{ac} coupling constants to account for optical and acoustic phonon interactions with electrons

for HfH₁₀) are credited to a large hydrogen-based DOS at E_F and strong coupling between electrons and optical phonons. A Bader charge analysis indicates 0.13e per H atom is transferred from Hf into antibonding H-based orbitals, lengthening H-H distances and increasing the H atom DOS at E_F .

Pentagonal motifs surface again in *Cmmm* ScH₁₂, with strips of edge-sharing H₅ pentagons running along the *c* direction that are spaced by Sc atoms¹⁰⁷ (Figure 4c). Short H-H distances between neighboring strips produce H₈ distorted octagons between them, with each Sc bracketed by one such H₈ octagon above and below. Such layered arrangements are reminiscent of the proposed high-pressure structure adopted by elemental H consisting of graphene-like sheets spaced by H₂ units, consistent with the especially high hydrogen content of this phase.

Between the remarkably low pressures of 75-100 GPa, *Cmcm* AcH₄ is predicted to be stable¹²¹. It is based on corrugated layers composed of H in distorted square nets with Ac atoms in between (Figure 4d). At 100 GPa, its estimated T_c extends up to a moderate 67 K¹²¹. An *Fddd* structure for ZrH₄ consists of atomistic hydrogen (Figure 4e), transitioning to the previously discussed *I4/mmm* structure above 210 GPa, while ZrH₆ with *Cmc2₁* symmetry – involving a mixture of atomistic hydrogen and H@H₃ units in a slightly pyramidal configuration – appears above 150 GPa until transitioning to either *I4/mmm* or *P2₁/c* symmetry at 275 GPa¹¹⁶. The *P2₁/c* structure, close in enthalpy to the tetragonally distorted *I4/mmm* ZrH₆ clathrate structure and mostly containing atomistic H, has an estimated T_c of 153 K at 295 K.

IV. TERNARY HYDRIDE MATERIALS

As described above, the phase diagrams of the various binary hydride systems have been thoroughly explored by theory, and experimental groups are making steady progress in synthesizing promising candidates. However, the high pres-

ures required to stabilize these phases leave the quest for a room-temperature atmospheric pressure superconductor incomplete. One way to accomplish this goal is to once again make use of the concept of chemical precompression by adding a third element into the mix. This third element can slot into void spaces present in a binary hydride framework, function as a dopant to raise or lower electron counts, or facilitate the stabilization of altogether new geometrical motifs unobserved in binary hydrides. The vast number of possible two-element-plus-hydrogen combinations is at once promising and daunting. Computationally, building a ternary convex hull is highly intensive, with many more possible stoichiometries to explore. As such, the current literature on ternary superconducting hydride materials is at times piecemeal, with systematic trends not yet identified, limiting the researcher's predictive power with regard to these phases. In what follows, we present a literature survey of ternary superconducting hydride phases that have been predicted thus far, grouping them into families where possible based on structural features or relationship to known binary prototypes. For brevity, we focus on phases with predicted T_c s over 100 K (see Table IV).

Several ternary phases based on partial substitution of a third element in a binary hydride structure have been studied theoretically. One example is the CaYH₁₂ phase, which contains the same metal/hydrogen arrangement as found in *Im $\bar{3}m$* CaH₆ and YH₆, but with the Ca and Y atoms in a B2 (CsCl-type) arrangement, reducing the overall symmetry to *Pm $\bar{3}m$* ¹³⁹. Of course, with an even larger unit cell, more complex coloring patterns can occur. For CaYH₁₂, a structure with *Fd $\bar{3}m$* symmetry, in which the Ca-Y sublattice displays a B1 (rock-salt) arrangement, possessed an even lower enthalpy and was dynamically stable above 170 GPa (Figure 5a). Although a full ternary convex hull was not constructed, the stability of these CaYH₁₂ phases was calculated relative to decomposition into CaH₆+YH₆ as well as CaH₄+YH₃+ $\frac{5}{2}$ H₂. The estimated T_c s of the two CaYH₁₂ phases were similar to those of the parent CaH₆ and YH₆ binaries.

A similar series of Sc-Ca-H ternary phases based on Sc/Ca mixing in binary $I4/mmm$ MH_4 and $Im\bar{3}m$ MH_6 phases have also been proposed, with the phase having the highest estimated T_c being $P4/mmm$ $ScCaH_8$ (212 K at 200 GPa)¹⁴⁰. Isotopic $YBaH_8$ is proposed to be stable to decomposition into BaH_2 and YH_6 above 50 GPa, with an estimated T_c of 49.6 K at 50 GPa, which increases to 89.4 K at 150 GPa¹⁴¹. Machine learning investigations on high- T_c materials created by substituting light elements such as Be, Li, Mg, and Na into YH_x phases prompted further searches into the Y-Mg-H system¹⁴². This led to a proposed metastable $Fd\bar{3}m$ $YMgH_{12}$ phase analogous to $Fd\bar{3}m$ $CaYH_{12}$ having an estimated T_c up to 189 K at 300 GPa¹⁴³, as well as a second $YMgH_{12}$ phase with $Cmmm$ symmetry (based on Ca and Y atoms in alternating layers along the c axis) with estimated T_c up to 153 K at 250 GPa.

With the extremely high T_c s of binary La and Y hydrides, a clear choice is to consider phases based on their mixture. A joint experimental/theoretical study¹⁴⁴ demonstrated both synthetic feasibility and high T_c , measuring T_c s of 253 K and 237 K for $(La/Y)H_{10}$ and $(La/Y)H_6$ respectively, with the latter being higher than measured for binary YH_6 . This result indicates the beneficial nature of La incorporation into the Y-H binary. The ternary convex hull was also calculated at 200 GPa. Notably, the only La-Y-H ternary that lay on it at 0 K was an $R\bar{3}m$ symmetry $LaYH_{20}$ structure, while increases in temperature eventually found La_2YH_{12} , La_4YH_{30} , $LaYH_{12}$, La_4YH_{50} , LaY_4H_{50} , and La_2YH_{18} (specific La/Y fractions for $(La/Y)H_4$, $(La/Y)H_6$, and $(La/Y)H_{10}$) all present on the convex hull, highlighting the importance of thermal effects and reinforcing the importance of considering metastable phases from the 0 K convex hull.

The above phases can all be constructed by partially substituting a third element onto one (or more) lattice sites in a known binary phase. However, as noted above, ternaries can also be created by adding a third element into void regions in a binary phase, thereby further tuning doping and leveraging the idea of “chemical precompression.” Two particularly fascinating materials based on this strategy are Li_2MgH_{16} , an electron-doped variant of MgH_{16} , and $LaBH_8$, a cousin of the high- T_c binary LaH_{10} .

Binary MgH_{16} , based on a network of Mg^{2+} cations in a lattice of $H_2^{\delta-}$ molecules, has been predicted to lie on the convex hull above 200 GPa¹²⁰. The donated electron density from the Mg atoms occupies the H_2 σ^* orbital, weakening the H_2 units – although not to the extent of forming fully extended networks as in the clathrate structures. The addition of lithium as an electron-doping agent was proposed to further perturb the H_2 units, resulting in the $P\bar{3}m1$ Li_2MgH_{16} structure, which lies only 20 meV/atom shy of the convex hull at 300 GPa.¹⁴⁵ In this structure, the electrons from Li destabilize the H-H bonds even further. An $Fd\bar{3}m$ phase, which overtakes the $P\bar{3}m1$ structure above 453 GPa, has fully dissociated the H_2 units to form clathrate cages (Figure 5b). This structure has a very large hydrogen-dominant electronic DOS at E_F . Because the estimated EPC parameter, $\lambda=3.35$, yields a T_c of 351 K at 300 GPa, this phase has been coined a “hot” superconductor¹⁴⁵. The structure remains dynamically stable

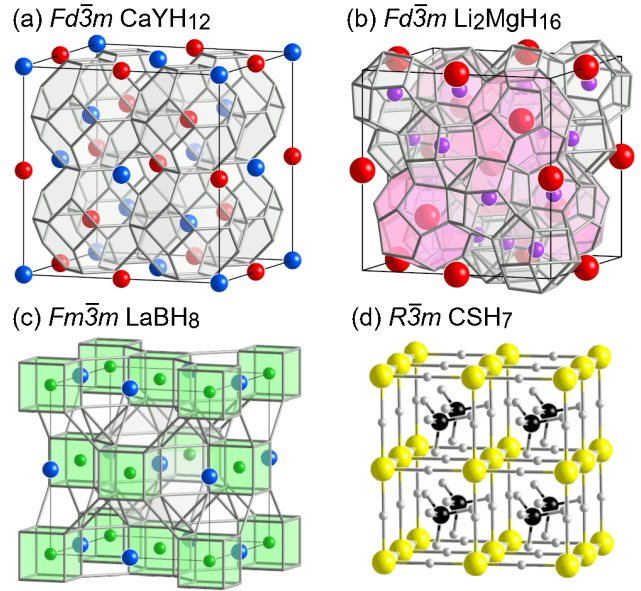


FIG. 5. Structures of selected ternary hydride superconducting phases. (a) $CaYH_{12}$ phase with $Fd\bar{3}m$ symmetry can be viewed as a colored variant of the $Im\bar{3}m$ MH_6 structure. (b) $Fd\bar{3}m$ Li_2MgH_{16} structure with interpenetrating $Li@H_{18}$ and $Mg@H_{28}$ clathrate lattices. (c) $Fm\bar{3}m$ $LaBH_8$ structure based on B intercalation into void spaces of an $Fm\bar{3}m$ MH_8 lattice. (d) $R\bar{3}m$ CSH_7 phase derived from methane substitution into cubic H_3S .

down to 250 GPa, where its estimated T_c increases further to 430-476 K. Here, electron doping through the addition of a third element changes the structural and electronic landscape of the phase, enhancing its superconducting properties.

Despite these substantial changes, adding Li to MgH_{16} does not drastically alter the pressure range of phase stability. The situation is somewhat different for $LaBH_8$, where boron atoms occupy H_8 cubes that are empty in structurally related LaH_{10} (Figure 5c).¹⁴⁶ Although it does not lie on the La-B-H ternary convex hull until 110 GPa, this phase maintains dynamic stability down to an impressive 40 GPa, suggesting that synthesis above 100 GPa then decompression could be a viable strategy to quench this phase to lower pressures. In contrast, LaH_{10} is not dynamically stable at pressures below 210 GPa.⁴⁴ Furthermore, the estimated T_c of $LaBH_8$ increases with decreasing pressure, going from ca. 42 K at 100 GPa up to ca. 126 K at 50 GPa.¹⁴⁶ This remarkable stability at low pressures is linked to the addition of boron atoms providing additional “chemical precompression” to the hydrogen lattice, thereby increasing the effective pressure even at lower external pressures. An additional study found that $LaBeH_8$ (in the same structure type) was dynamically stable down to 50 GPa, where its T_c was estimated to be 191 GPa¹⁴⁷. In addition to the La-B-H and La-Be-H structures, $LaAlH_8$, $CaBH_8$, and $YBeH_8$ were also found to be dynamically stable at pressures below 100 GPa and $LaBeH_8$, $CaBH_8$, $YBeH_8$, and $SrBH_8$ (dynamically stable above 210 GPa) were all found to lie on the convex hull¹⁴⁷. Finally, whereas the previous XYH_8 phases involve placement

of Be or B into H_8 cubes in an MH_8 hydrogen framework, another possibility for this structure is presented by KB_2H_8 ¹⁴⁸ and LaC_2H_8 ¹⁴⁹, in which B and C are respectively placed into the H_4 tetrahedral vacancies of an MH_8 structure, resulting in a “colored” version of the LaH_{10} lattice. KB_2H_8 remains dynamically stable down to 12 GPa, where its T_c is estimated to be 134-146 K¹⁴⁸. LaC_2H_8 is dynamically stable above 70 GPa, with an estimated T_c of 69 K, increasing to 140 K at 250 GPa¹⁴⁹. As such, the XYH_8 and XY_2H_8 families, with a hydrogenic lattice stabilized to low pressure by scaffolding atoms, could be a useful vector for further investigations.

The $B@H_8$ cubes featured in several of the aforementioned phases are one instance of $B@H_n$ polyhedra prevalent in ternary superconducting systems. Other examples are $B@H_6$ octahedra found in Li_2BH_6 ¹⁵⁰, $CaBH_6$, and $Ca_2B_2H_{13}$ ¹⁵¹. In the former, the $B@H_6$ octahedra are arranged in an fcc lattice intercalated with Li atoms, resulting in an $Fm\bar{3}m$ structure that is stable down to 100 GPa. Its T_c has been estimated to be 98 K at 100 GPa, with most contributions arising from atomic vibrations of intermediate frequencies. $CaBH_6$ with $Pa\bar{3}$ symmetry is metastable by ca. 100 meV/atom above 100 GPa, while $Ca_2B_2H_{13}$ has Pm symmetry and lies on the convex hull above 275 GPa. At 300 GPa, the estimated T_c of $CaBH_6$ is 97-119 K, although little pressure dependence is observed down to 100 GPa, while that of $Ca_2B_2H_{13}$ is 75-89 K at 300 GPa. Since they lie closer to E_F than in other alkali and alkaline earth metals, the interactions – or lack thereof – of the Ca d orbitals with the rest of the atoms are postulated to be key to the superconducting properties of the Ca-B-H phases. A metastable $LaBH_{17}$ stoichiometry phase was identified alongside $LaBH_8$ ¹⁵², with La atoms encapsulated in clathrate-like H_{32} cages interspersed with B_2H_{10} units.

A third fruitful family of ternary hydrides are those based on covalent networks such as those found in H_3S – the first high T_c hydride to be synthesized.² Key to its record breaking superconducting properties is the presence of a pair of van Hove singularities (vHs) bracketing E_F . Since doping H_3S could shift E_F to place it more directly at the peak in the DOS created by the vHs – increasing the EPC and concomitant T_c – several studies have investigated the effect of adding a third element into the H_3S framework. One of these examined the effects of replacing half of the sulfur atoms with selenium, finding three dynamically stable H_6SSe structures at 200 GPa, with $Pm\bar{3}m$, $Cmmm$, and $Fd\bar{3}m$ symmetries arising from different S/Se substitution patterns¹⁵⁴. At this pressure, their T_c s were predicted to be 196, 181, and 115 K respectively, all lower than the 246 K estimated for $Im\bar{3}m$ H_3S at 200 GPa. Other thermodynamically stable S/Se compositions were explored using the cluster expansion method, all of which had greatly reduced estimated T_c s compared to cubic H_3S and H_3Se ⁵⁴.

Considering other ternary H_3S -based systems, studies using the virtual crystal approximation (VCA)^{155,156,163} found that small amounts of phosphorus, carbon or silicon doping could shift E_F sufficiently to increase the T_c of the model $H_3S_{(1-x)}Z_x$ phase to 280 K ($Z=P$)¹⁵⁵, 289 K ($Z=C$)¹⁵⁶ and 283 K ($Z=Si$)¹⁵⁶. In fact, a “carbonaceous sulfur hydride” phase was recently reported to be the world’s first room-

temperature superconductor⁸, although the conclusions of the manuscript have been called into question¹⁶⁴⁻¹⁶⁶. Thus far, the C-S-H phase has eluded characterization, given the experimental difficulty of obtaining structural information for light element systems and in particular those under pressure. Further complicating the matter, the aforementioned VCA results do not account for the local bonding and structural modifications that result from substituting an actual dopant atom into the H_3S lattice¹⁶⁶, and further exploration is required – and ongoing – to determine the precise structural motifs within the carbonaceous sulfur hydride superconductor^{167,168}.

Prior to the experimental observation of the carbonaceous sulfur hydride system, two groups identified promising metastable C-S-H phases based on methane intercalation into an H_3S lattice^{157,158} (Figure 5d). The CSH_7 stoichiometry was especially promising, and various dynamically stable phases that differed via rotation of the methane molecules were identified. The phases with the highest predicted T_c s were $I\bar{4}3m$ CSH_7 (181 K at 100 GPa¹⁵⁷) and $R\bar{3}m$ CSH_7 (181-194 K at 150 GPa¹⁵⁸). However, it is uncertain if these structural motifs are present in the C-S-H phase synthesized in Ref. 8. For example, recent experimental investigations^{169,170} suggest the formation of an Al_2Cu -based structure within the C-S-H system under pressure, rather than a phase derived from the $Im\bar{3}m$ H_3S structure.

One of the most well-known structures among intermetallic superconductors is the A15 phase adopted by Nb_3Sn ¹² ($T_c=18$ K). A ternary $Pm\bar{3}$ $LiPH_6$ phase comprised of a colored A15 lattice was predicted above 250 GPa¹⁰². A large peak in the DOS just below E_F was observed, with an estimated T_c as high as 167 K at 200 GPa. ELF analysis indicated that the H atoms are not bound to one another, with H-H distances of 1.14 Å at 300 GPa. In addition to a large H-based contribution to the DOS at E_F , the low atomic mass of Li was also thought to enhance T_c , especially upon comparison with previously identified isotypic $MgSiH_6$ and $MgGeH_6$ phases with much lower T_c s (63 K¹⁷¹ and 67 K¹⁷²). Additional investigation of the Li-P-H system showed that the inclusion of ZPE effects renders several phases including $LiPH_6$ metastable. From 250-400 GPa, a $R\bar{3}$ phase with LiP_2H_{14} stoichiometry was found, built from $P@H_9$ polyhedra and interstitial Li and H atoms¹⁶¹. At 230 GPa this phase reaches an estimated $T_c=169$ K, with the majority of the EPC resulting from H-H stretching modes. Without performing full CSP searches, Na and Be were substituted for Li in this structure to examine the role of atomic mass on T_c , finding enhancement at high pressures with NaP_2H_{14} having $T_c=159$ K at 400 GPa (relative to 90 K for LiP_2H_{14} at this pressure).

With the high T_c s of the CaH_6 and H_3S phases in mind, the Ca-S-H system was investigated. In addition to a number of semiconducting phases based on H_2 molecules in a Ca/S lattice, a $P\bar{6}m2$ $CaSH_3$ structure with stacked alternating S-H honeycomb nets and CaH_2 layers was found to lie 3-28 meV/atom above the convex hull in the 150-250 GPa pressure range, and on the hull at 300 GPa¹⁵⁹. Two vHs were found to lie bracket E_F resulting in a T_c as high as 94-101 K at 128 GPa. It was proposed that replacing Ca by other alkaline earth metals, and S with heavier chalcogens could lead to

TABLE IV. Superconducting properties of select ternary hydrides (Figure 5).

Structure (space group)	Pressure (GPa)	λ	μ^*	T_c
CaYH ₁₂ ¹³⁹ (<i>Pm</i> $\bar{3}m$) ^e	200	2.06	0.13-0.1	196-215 ^{a,f} , 233-248 ^b
CaYH ₁₂ ¹³⁹ (<i>Fd</i> $\bar{3}m$)	200	2.20	0.13-0.1	207-226 ^{a,f} , 243-258 ^b
ScCaH ₈ ¹⁴⁰ (<i>P4/mmm</i>)	160	1.62	0.1	130.2 ^{a,f}
ScCaH ₈ ¹⁴⁰ (<i>P4/mmm</i>)	200	1.89	0.1	212.1 ^{a,f}
ScCaH ₁₂ ¹⁴⁰ (<i>Pm</i> $\bar{3}m$)	160	1.80	0.1	174.9 ^{a,f}
ScCaH ₁₂ ¹⁴⁰ (<i>Pm</i> $\bar{3}m$)	300	1.68	0.1	193.2 ^{a,f}
YMgH ₈ ¹⁴³ (<i>P4/mmm</i>)	300	1.63	0.13-0.1	115-125 ^a
YMgH ₁₂ ¹⁴³ (<i>Fd</i> $\bar{3}m$) ^e	300	1.81	0.13-0.1	175-189 ^a
YMgH ₁₂ ¹⁴³ (<i>Cmmm</i>)	250	1.66	0.13-0.1	141-153 ^a
La ₂ YH ₁₈ ¹⁴⁴ (<i>Pm</i> $\bar{3}m$)	180	2.74 ^c	0.15-0.1	197-229 ^a , 248-270 ^b
LaYH ₁₂ ¹⁴⁴ (<i>Pm</i> $\bar{3}m$)	180	2.82	0.15-0.1	176-203 ^a , 223-241 ^b
La ₄ YH ₃₀ ¹⁴⁴ (<i>Pm</i> $\bar{3}m$)	180	2.68 ^c	0.15-0.1	206-237 ^a , 245-265 ^b
LaYH ₂₀ ¹⁴⁴ (<i>R</i> $\bar{3}m$)	180	3.87	0.15-0.1 (0.2)	232-266 ^a , 281-300 (266) ^b
Li ₂ MgH ₁₆ ¹⁴⁵ (<i>Fd</i> $\bar{3}m$) ^e	250	4.0	0.16-0.1	430-473 ^b
LaBH ₈ ¹⁴⁶ (<i>Fm</i> $\bar{3}m$)	50	1.54	0.09	122 ^b , 126 ^{b,d}
LaBH ₈ ¹⁵³ (<i>Fm</i> $\bar{3}m$)	50	2.29	0.13-0.1	102-108 ^a , (154, $\mu^* = 0.1$) ^b
LaBH ₁₇ ¹⁵² (<i>I222</i>) ^e	300	3.3	0.1	180 ^b
KB ₂ H ₈ ¹⁴⁸ (<i>Fm</i> $\bar{3}m$)	12	2.99	0.15-0.1	134-146 ^b
LaC ₂ H ₈ ¹⁴⁹ (<i>Fm</i> $\bar{3}m$)	250	1.63	0.1	107 ^a , 140 ^b
Li ₂ BH ₆ ¹⁵⁰ (<i>Fm</i> $\bar{3}m$)	100	0.94	0.1	98 ^a
CaBH ₆ ¹⁵¹ (<i>Pa</i> $\bar{3}$)	100	1.93	0.15-0.1	100-114 ^a
Ca ₂ B ₂ H ₁₃ ¹⁵¹ (<i>Pm</i>)	300	1.37	0.15-0.1	75-89 ^a
H ₆ SSe ¹⁵⁴ (<i>Pm</i> $\bar{3}m$)	200	1.76	0.1	196 ^b
H ₆ SSe ¹⁵⁴ (<i>Cmmm</i>)	200	1.60	0.1	181 ^b
H ₆ SSe ¹⁵⁴ (<i>Fd</i> $\bar{3}m$)	200	0.99	0.1	115 ^b
H ₃ S _(1-x) P _x ^{g,155} (<i>Im</i> $\bar{3}m$)	250	2.44	0.1	280 ^{a,f}
H ₃ S _(1-x) C _x ^{g,156} (<i>Im</i> $\bar{3}m$)	260	2.43 ^h	0.15-0.1	289 ^{a,f}
H ₃ S _(1-x) Si _x ^{g,156} (<i>Im</i> $\bar{3}m$)	230	2.46 ^h	0.15-0.1	283 ^{a,f}
CSH ₇ ¹⁵⁷ (<i>I</i> $\bar{4}3m$)	100	3.64	0.13-0.1	114-126 ^a , 173-181 ^b
CSH ₇ ¹⁵⁸ (<i>R</i> $\bar{3}m$)	150	2.47	0.13-0.1	143-152 ^a , 181-194 ^b
CSH ₇ ¹⁵⁸ (<i>Pnma</i>)	150	3.06	0.13-0.1	116-122 ^a , 157-170 ^b
CSH ₇ ¹⁵⁸ (<i>Cm</i>)	100	1.20	0.13-0.1	86-98 ^a , 97-108 ^b
H ₆ SSe ¹⁵⁴ (<i>Pm</i> $\bar{3}m$)	200	1.76	0.1	246 ^b
H ₆ SSe ¹⁵⁴ (<i>Cmmm</i>)	200	1.60	0.1	196 ^b
H ₆ SSe ¹⁵⁴ (<i>Fd</i> $\bar{3}m$)	200	0.99	0.1	115 ^b
CaSH ₃ ¹⁵⁹ (<i>P</i> $\bar{6}m2$)	128	1.64	0.13-0.1	71-78 ^a , 94-101 ^b
MgCH ₄ ¹⁶⁰ (<i>P4/nmm</i>)	105	1.49 ⁱ	0.1	121 ^a
LiPH ₆ ¹⁰² (<i>Pm</i> $\bar{3}$)	200 ^e	1.62	0.13-0.1	125.3-136.5 ^a , 149.6-167.3 ^{a,f}
LiP ₂ H ₁₄ ¹⁶¹ (<i>R</i> $\bar{3}$)	230	1.69	0.16-0.1	116-143 ^a , 138-169 ^b
NaP ₂ H ₁₄ ¹⁶¹ (<i>R</i> $\bar{3}$)	400	1.45	0.1	111-139 ^a , 130-159 ^b
NSiH ₁₁ ¹⁶² (<i>P2</i> ₁ / <i>m</i>)	300	1.29	0.13-0.1	98-110 ^a

^a T_c was calculated using the Allen-Dynes modified McMillan equation (Equation 5)

^b T_c was calculated by numerical solution of the Eliashberg equations

^c Values obtained from the interpolation method

^d Values calculated using fully anisotropic Migdal-Eliashberg theory

^e Metastable at this pressure

^f T_c was calculated using the Allen-Dynes modified McMillan equation with strong coupling and shape corrections (Equations 7 and 8)

^g Calculated within the virtual crystal approximation (VCA)

^h Values estimated from Figure 2 in Ref.156

ⁱ Values estimated from Figure 4 in Ref.160

other superconducting materials in this structure type.

In analogy to the chemical precompression strategy to metallize hydrogen, Mg-doping was proposed as a way to metallize methane, resulting in the prediction of a *P4/nmm*-symmetry MgCH₄ phase stable above 75 GPa, where it overtakes a semiconducting *Pban* structure¹⁶⁰. A maximum T_c of

121 K was predicted at 105 GPa.

With the aim of incorporating large amounts of H into the system, prompted by the report of NH₄ and NH₇ structures¹⁷³, N-Si-H ternaries were explored at 300 GPa¹⁶². While all candidate ternary structures were metastable, the lowest-lying of these was *P2*₁/*m* NSiH₁₁, lying 42 meV/atom above the con-

vex hull. Weakly bound H_2 units account for most of the hydrogen in the phase, with some atomic hydrogen covalently linked to nitrogen. At 300 GPa, $NSiH_{11}$ has an estimated T_c of 98-110 K, with the interaction of N atoms with the Si-H network leading to almost half of the EPC.

V. CONCLUSION AND OUTLOOK

Less than a decade after the theoretical prediction of high temperature superconductivity with a T_c up to 220-235 K in a clathrate-like CaH_6 phase⁴² and the measurement of superconductivity at 203 K in H_3S^2 , the landscape of superconducting materials with high hydrogen content has been heavily explored – for binary phases, primarily. The nature of the hydrogenic sublattice in these structures has been found to heavily influence their superconducting properties, with high T_c s belonging to phases in which H_2 units have been disrupted, resulting in elongated H-H distances and/or multi-centered bonds between hydrogen and another element. Exemplars include phases with clathrate-like three-dimensional networks of loosely bound hydrogen and the family of MH_4 phases that mix atomic and H_2 units. In the latter, T_c is further correlated with H-H distance in the molecular units, which increases with larger metal atoms, and increased electron transfer from those metal atoms that results in populating the antibonding states of the H network. Anomalously high T_c values also crop up in phases with more unique H motifs, including “pentagraphene-like” units in ScH_{10} . The large values for the electron-phonon coupling constants that result in high T_c s are associated with an electronic structure easily perturbed by atomic vibrations as well as a large amount of H-based states near E_F ^{174,175}. With the vibrations of the hydrogen lattice generally spread across a wide range of frequencies, this effect is strongest for the phases with clathrate-like lattices and weaker for phases based on $H_2^{\delta-}$ units, such as the $ThCr_2Si_2$ MH_4 family.

Ternary hydrides – or quaternary and higher – represent a new frontier where the search is on for superconducting materials that maintain dynamic stability to lower and lower pressures^{147,152,153}. Thus far, investigation of ternary phase diagrams remains somewhat piecemeal, with only a few full convex hulls calculated^{37,102,144,146,147,151,161}. The combinatorial possibilities for three elements generate a massive phase space that cannot be thoroughly investigated – whether by current experimental or theoretical techniques – on a reasonable timescale. The goal for the theoretician is thus threefold: to identify promising systems for more detailed studies³⁷, as well as to develop new methods and protocols for rapid calculations, and the analysis of the large amount of data generated during the construction of full ternary convex hulls. Moreover, it is expected that entropic effects, currently neglected, will become key in the stabilization of multicomponent systems¹⁷⁶.

Towards the former goal, a common strategy is to consider substitutions of a third element into a known binary hydride, exemplified by the mixed La/Y hydrides recently shown to form¹⁴⁴ and the MXH_8 phases from intercalation

of a third element into a common MH_8 skeleton^{146,147,153}. Systematic studies to identify trends in binary hydrides can identify plausible third “alloying” elements or locations in a binary lattice susceptible to substitution³⁹. After selecting promising systems, strategies to more rapidly process the computations required for crystal structure prediction include using interatomic force fields for local optimizations rather than full DFT^{69,177,178}. Machine learning techniques can expedite the generation of useful force fields and in some cases have already been integrated into CSP packages^{67,68}. The feedback loop of experimental and theoretical investigation into superconducting hydrides, then, may explore strange new ternary systems, seek out new structural motifs, and boldly discover superconducting phases – at pressures and temperatures where none have been found before.

ACKNOWLEDGMENTS

We acknowledge the NSF (DMR-1827815) for financial support. K. P. H. thanks the US Department of Energy, National Nuclear Security Administration, through the Chicago-DOE Alliance Center under Cooperative Agreement Grant No. DE-NA0003975 for financial support.

REFERENCES

- ¹N. W. Ashcroft, Phys. Rev. Lett. **21**, 1748 (1968).
- ²A. P. Drozdov, M. I. Erements, I. A. Troyan, V. Ksenofontov, and S. I. Shylin, Nature **525**, 73 (2015).
- ³M. Somayazulu, M. Ahart, A. K. Mishra, Z. M. Geballe, M. Baldini, Y. Meng, V. V. Struzhkin, and R. J. Hemley, arXiv:1808.07695 (2018).
- ⁴A. P. Drozdov, P. P. Kong, V. S. Minkov, S. P. Besedin, M. A. Kuzovnikov, S. Mozaffari, L. Balicas, F. F. Balakirev, D. E. Graf, V. B. Prakapenka, E. Greenberg, D. A. Knyazev, M. Tkacz, and M. I. Erements, Nature **569**, 528 (2019).
- ⁵E. Snider, N. Dasenbrock-Gammon, R. McBride, X. Wang, N. Meyers, K. V. Lawler, E. Zurek, A. Salamat, and R. P. Dias, Phys. Rev. Lett. **126**, 117003 (2021).
- ⁶P. Kong, V. S. Minkov, M. A. Kuzovnikov, A. P. Drozdov, S. P. Besedin, S. Mozaffari, L. Balicas, F. F. Balakirev, V. B. Prakapenka, S. Chariton, D. A. Knyazev, E. Greenberg, and M. I. Erements, Nature Commun. **12**, 5075 (2021).
- ⁷I. A. Troyan, D. V. Semenok, A. G. Kvashnin, A. V. Sadakov, O. A. Sobolevskiy, V. M. Pudalov, A. G. Ivanova, V. B. Prakapenka, E. Greenberg, A. G. Gavriluk, I. S. Lyubutin, V. V. Struzhkin, A. Bergara, I. Errea, R. Bianco, M. Calandra, F. Mauri, L. Monacelli, R. Akashi, and A. R. Oganov, Adv. Mater. **33**, 2006832 (1 (2021)).
- ⁸E. Snider, N. Dasenbrock-Gammon, R. McBride, M. Debessai, H. Vindana, K. Vencatasamy, K. V. Lawler, A. Salamat, and R. P. Dias, Nature **586**, 373 (2020).
- ⁹K. Conder, Supercond. Sci. Technol. **29**, 080502 (2016).
- ¹⁰E. Wigner and H. B. Huntington, J. Chem. Phys. **3**, 764 (1935).

- ¹¹In a footnote Wigner and Huntington say that “It was J. D. Bernal who first put forward the view that all substances go over under very high pressure into metallic or valence lattices.”
- ¹²B. T. Matthias, T. H. Geballe, S. Geller, and E. Corenzwit, *Phys. Rev.* **95**, 1435 (1954).
- ¹³J. R. Gavaler, *Appl. Phys. Lett.* **23**, 480 (1973).
- ¹⁴M. K. Wu, J. R. Ashburn, C. J. Torng, P. H. Hor, R. L. Meng, L. Gao, Z. J. Huang, Y. Q. Wang, and C. W. Chu, *Phys. Rev. Lett.* **58**, 908 (1987).
- ¹⁵C. Narayana, H. Luo, J. Orloff, and A. L. Ruoff, *Nature* **393**, 46 (1998).
- ¹⁶P. Loubeyre, F. Occelli, and R. LeToullec, *Nature* **416**, 613 (2002).
- ¹⁷C. S. Zha, Z. Liu, M. Ahart, R. Boehler, and R. J. Hemley, *Phys. Rev. Lett.* **110**, 217402 (2013).
- ¹⁸M. I. Erements and I. A. Troyan, *Nat. Mater.* **10**, 927 (2011).
- ¹⁹R. T. Howie, C. L. Guillaume, T. Scheler, A. F. Goncharov, and E. Gregoryanz, *Phys. Rev. Lett.* **108**, 125501 (2012).
- ²⁰P. Dalladay-Simpson, R. T. Howie, and E. Gregoryanz, *Nature* **529**, 63 (2016).
- ²¹N. W. Ashcroft, *Phys. Rev. Lett.* **92**, 187002 (2004).
- ²²J. Nagamatsu, N. Nakagawa, T. Muranaka, Y. Zenitani, and J. Akimitsu, *Nature* **410**, 63 (2001).
- ²³J. Feng, W. Grochala, T. Jaroń, R. Hoffmann, A. Bergara, and N. W. Ashcroft, *Phys. Rev. Lett.* **96**, 017006 (2006).
- ²⁴C. J. Pickard and R. J. Needs, *Phys. Rev. Lett.* **97**, 045504 (2006).
- ²⁵Y. Yao, J. S. Tse, Y. Ma, and K. Tanaka, *EPL* **78**, 37003 (2007).
- ²⁶D. Kurzydłowski and W. Grochala, *Acta Phys. Pol. A* **119**, 895 (2011).
- ²⁷M. Martinez-Canales, A. Bergara, J. Feng, and W. Grochala, *J. Phys. Chem. Solids* **67**, 2095 (2006).
- ²⁸G. Gao, A. R. Oganov, A. Bergara, M. Martinez-Canales, T. Cui, T. Iitaka, Y. Ma, and G. Zou, *Phys. Rev. Lett.* **101**, 107002 (2008).
- ²⁹M. Miao, Y. Sun, E. Zurek, and H. Lin, *Nat. Rev. Chem.* **508-527**, 4 (2020).
- ³⁰W. Grochala, R. Hoffmann, J. Feng, and N. W. Ashcroft, *Angew. Chem. Int. Ed.* **46**, 3620 (2007).
- ³¹E. Zurek and W. Grochala, *Phys. Chem. Chem. Phys.* **17**, 2917 (2015).
- ³²W. Zhang, A. R. Oganov, A. F. Goncharov, Q. Zhu, S. E. Boulfelfel, A. O. Lyakhov, E. Stavrou, M. Somayazulu, V. B. Prakapenka, and Z. Konôpková, *Science* **342**, 1502 (2013).
- ³³A. Shamp and E. Zurek, *J. Phys. Chem. Lett.* **6**, 4067 (2015).
- ³⁴E. Zurek and T. Bi, *J. Chem. Phys.* **150**, 050901 (1 (2019)).
- ³⁵T. Bi, N. Zarifi, T. Terpstra, and E. Zurek, in *Reference module in chemistry, molecular sciences and chemical engineering*, edited by J. Reedijk (Elsevier, Waltham, MA, 2019) pp. 1–36.
- ³⁶J. A. Flores-Livas, L. Boeri, A. Sanna, G. Profeta, R. Arita, and M. Erements, *Phys. Rep.* **856**, 1 (2020).
- ³⁷M. J. Hutcheon, A. M. Shipley, and R. J. Needs, *Phys. Rev. B* **101**, 144505 (2020).
- ³⁸L. Boeri, R. G. Hennig, P. J. Hirschfeld, G. Profeta, A. Sanna, E. Zurek, W. E. Pickett, M. Amsler, R. Dias, and M. Erements, *J. Phys. Condens. Matter* **Just Accepted** (2021).
- ³⁹A. M. Shipley, M. J. Hutcheon, R. J. Needs, and C. J. Pickard, *Phys. Rev. B* **104**, 054501 (2021).
- ⁴⁰C. M. Pépin, G. Geneste, A. Dewaele, M. Mezouar, and P. Loubeyre, *Science* **357**, 382 (2017).
- ⁴¹H. Xie, Y. Yao, X. Feng, D. Duan, H. Song, Z. Zhang, S. Jiang, S. A. T. Redfern, V. Z. Kresin, C. J. Pickard, and T. Cui, *Phys. Rev. Lett.* **125**, 217001 (2020).
- ⁴²H. Wang, J. S. Tse, K. Tanaka, T. Iitaka, and Y. Ma, *Proc. Natl. Acad. Sci. U.S.A.* **109**, 6463 (2012).
- ⁴³F. Peng, Y. Sun, C. J. Pickard, R. J. Needs, Q. Wu, and Y. Ma, *Phys. Rev. Lett.* **119**, 107001 (2017).
- ⁴⁴H. Liu, I. I. Naumov, R. Hoffmann, N. W. Ashcroft, and R. J. Hemley, *Proc. Natl. Acad. Sci. U.S.A.* **114**, 6990 (2017).
- ⁴⁵J. M. McMahon and D. M. Ceperley, *Phys. Rev. B* **84**, 144515 (2011).
- ⁴⁶Y. Ma, M. Erements, A. R. Oganov, Y. Xie, I. Trojan, S. Medvedev, A. O. Lyakhov, M. Valle, and V. Prakapenka, *Nature* **458**, 182 (2009).
- ⁴⁷Y. Wang and Y. Ma, *J. Chem. Phys.* **140**, 040901 (2014).
- ⁴⁸R. J. Needs and C. J. Pickard, *APL Mater.* **4**, 053210 (2016).
- ⁴⁹E. Zurek, in *Reviews in Computational Chemistry*, Vol. 29, edited by A. L. Parrill and K. B. Lipkowitz (John Wiley & Sons, Inc., Hoboken, New Jersey, 2016) pp. 274–326.
- ⁵⁰P. Avery, X. Wang, C. Oses, E. Gossett, D. M. Proserpio, C. Toher, S. Curtarolo, and E. Zurek, *npj Comput. Mater.* **5**, 89 (2019).
- ⁵¹A. Shamp and E. Zurek, *Nov. Supercond. Mater.* **3**, 14 (2017).
- ⁵²S. Goedecker, *J. Chem. Phys.* **120**, 9911 (2004).
- ⁵³M. Amsler and S. Goedecker, *J. Chem. Phys.* **133**, 224104 (2010).
- ⁵⁴M. Amsler, *Phys. Rev. B* **99**, 060102(R) (2019).
- ⁵⁵S. Kirkpatrick, C. D. Gelatt, and M. P. Vecchi, *Science* **220**, 671 (1983).
- ⁵⁶A. Laio and M. Parrinello, *Proc. Natl. Acad. Sci.* **99**, 12562 (2002).
- ⁵⁷J. Sun, D. D. Klug, and R. Martoňák, *J. Chem. Phys.* **130**, 194512 (2009).
- ⁵⁸S. T. Call, D. Y. Zubarev, and A. I. Boldyrev, *J. Comput. Chem.* **28**, 1177 (2007).
- ⁵⁹Y. Wang, J. Lv, L. Zhu, S. Lu, K. Yin, Q. Li, H. Wang, L. Zhang, and Y. Ma, *J. Phys. Condens. Matter* **27**, 203203 (2015).
- ⁶⁰A. R. Oganov, A. O. Lyakhov, and M. Valle, *Acc. Chem. Res.* **44**, 227 (2011).
- ⁶¹D. C. Lonie and E. Zurek, *Comput. Phys. Commun.* **182**, 372 (2011).
- ⁶²C. J. Pickard and R. J. Needs, *phys. status solidi (b)* **246**, 536 (2009).
- ⁶³C. J. Pickard and R. J. Needs, *J. Phys.: Condens. Matter* **23**, 053201 (2011).

- ⁶⁴Z. Falls, P. Avery, X. Wang, K. P. Hilleke, and E. Zurek, *J. Phys. Chem. C* **125**, 1601 (2021).
- ⁶⁵J. P. Perdew, K. Burke, and M. Ernzerhof, *Phys. Rev. Lett.* **77**, 3865 (1996).
- ⁶⁶S. Q. Wu, M. Ji, C. Z. Wang, M. C. Nguyen, X. Zhao, K. Umemoto, R. M. Wentzcovitch, and K. M. Ho, *J. Phys.: Condens. Matter* **26**, 035402 (2014).
- ⁶⁷Q. Tong, L. Xue, J. Lv, Y. Wang, and Y. Ma, *Faraday Discuss.* **211**, 31 (2018).
- ⁶⁸E. V. Podryabinkin, R. V. Tikhonov, A. V. Shapeev, and A. R. Oganov, *Phys. Rev. B* **99**, 064114 (2019).
- ⁶⁹C. Hong, J. M. Choi, W. Jeong, S. Kang, S. Ju, K. Lee, J. Jung, Y. Youn, and S. Han, *Phys. Rev. B* **102**, 224104 (2020).
- ⁷⁰D. Kurzydowski, M. Derzsi, E. Zurek, and W. Grochala, *Chem. Eur. J.* **27**, 5536 (2021).
- ⁷¹T. Kaewmaraya, D. Y. Kim, S. Lebègue, C. J. Pickard, R. J. Needs, and R. Ahuja, *Phys. Rev. B* **84**, 092101 (2011).
- ⁷²V. L. Deringer, R. P. Stoffel, and R. Dronskowski, *Cryst. Growth Des.* **14**, 871 (2014).
- ⁷³E. I. Román-Román and C. M. Zicovich-Wilson, *Chem. Phys. Lett.* **619**, 109 (2015).
- ⁷⁴A. Hermann, M. Derzsi, W. Grochala, and R. Hoffmann, *Inorg. Chem.* **55**, 1278 (2016).
- ⁷⁵D. V. Semenok, D. Zhou, A. G. Kvashnin, X. Huang, M. Galasso, I. A. Kruglov, A. G. Ivanova, A. G. Gavriluk, W. Chen, N. V. Tkachenko, A. I. Boldyrev, I. Troyan, A. R. Oganov, and T. Cui, *J. Phys. Chem. Lett.* **12**, 32 (2021).
- ⁷⁶J. Zhao, B. Ao, S. Li, T. Gao, and X. Ye, *J. Phys. Chem. C* **124**, 7361 (2020).
- ⁷⁷Y. L. Hai, N. Lu, H. L. Tian, M. J. Jiang, W. Yang, W. J. Li, X. W. Yan, C. Zhang, X. J. Chen, and G. H. Zhong, *J. Phys. Chem. C* **125**, 3640 (2021).
- ⁷⁸A. V. Krukau, O. A. Vydrov, A. F. Izmaylov, and G. E. Scuseria, *J. Chem. Phys.* **125**, 224106 (2006).
- ⁷⁹I. Errea, M. Calandra, C. J. Pickard, J. Nelson, R. J. Needs, Y. Li, H. Liu, Y. Zhang, Y. Ma, and F. Mauri, *Phys. Rev. Lett.* **114**, 157004 (2015).
- ⁸⁰I. Errea, F. Belli, L. Monacelli, A. Sanna, T. Koretsune, T. Tadano, R. Bianco, M. Calandra, R. Arita, F. Mauri, and J. A. Flores-Livas, *Nature* **578**, 66 (2020).
- ⁸¹P. Hou, F. Belli, R. Bianco, and I. Errea, *Phys. Rev. B* **103**, 134305 (2021).
- ⁸²W. Sun, S. T. Dacek, S. P. Ong, G. Hautier, A. Jain, W. D. Richards, A. C. Gamst, K. A. Persson, and G. Ceder, *Sci. Adv.* **2**, e1600225 (2016).
- ⁸³H. K. Onnes, *Proc. K. Ned. Akad. Wet. B* **14**, 113 (1911).
- ⁸⁴E. Maxwell, *Phys. Rev.* **78**, 477 (1950).
- ⁸⁵C. A. Reynolds, R. Serin, W. H. Wright, and L. B. Nesbitt, *Phys. Rev.* **78**, 487 (1950).
- ⁸⁶H. Fröhlich, *Phys. Rev.* **79**, 845 (1950).
- ⁸⁷J. Bardeen, L. N. Cooper, and J. R. Schrieffer, *Phys. Rev.* **106**, 162 (1957).
- ⁸⁸J. Bardeen, L. N. Cooper, and J. R. Schrieffer, *Phys. Rev.* **108**, 1175 (1957).
- ⁸⁹D. Duan, Y. Liu, F. Tian, D. Li, X. Huang, Z. Zhao, H. Yu, B. Liu, W. Tian, and T. Cui, *Sci. Rep.* **4**, 6968 (2014).
- ⁹⁰A. P. Drozdov, V. S. Minkov, S. P. Besedin, P. P. Kong, M. A. Kuzovnikov, D. A. Knyazev, and M. I. Erements, arXiv:1808.07039 (2018).
- ⁹¹G. M. Eliashberg, *Sov. Phys. JETP* **11**, 696 (1960).
- ⁹²W. L. McMillan, *Phys. Rev.* **167**, 331 (1968).
- ⁹³P. B. Allen and R. C. Dynes, *Phys. Rev. B* **12**, 905 (1975).
- ⁹⁴R. C. Dynes, *Solid State Commun.* **10**, 615 (1972).
- ⁹⁵P. Giannozzi, S. Baroni, N. Bonini, M. Calandra, R. Car, C. Cavazzoni, D. Ceresoli, G. L. Chiarotti, M. Cococcioni, I. Dabo, A. D. Corso, S. de Gironcoli, S. Fabris, G. Fratesi, R. Gebauer, U. Gerstmann, C. Gougoussis, A. Kokalj, M. Lazzeri, L. Martin-Samos, N. Marzari, F. Mauri, R. Mazzarello, S. Paolini, A. Pasquarello, L. Paulatto, C. Sbraccia, S. Scandolo, G. Sclauzero, A. P. Seitsonen, A. Smogunov, P. Umari, and R. M. Wentzcovitch, *Journal of Physics: Condensed Matter* **21**, 395502 (2009).
- ⁹⁶X. Gonze, B. Amadon, G. Antonius, F. Arnardi, L. Baguet, J.-M. Beuken, J. Bieder, F. Bottin, J. Bouchet, E. Bousquet, N. Brouwer, F. Bruneval, G. Brunin, T. Cavignac, J.-B. Charraud, W. Chen, M. Côté, S. Cottenier, J. Denier, G. Geneste, P. Ghosez, M. Giantomassi, Y. Gillet, O. Gingras, D. R. Hamann, G. Hautier, X. He, N. Helbig, N. Holzwarth, Y. Jia, F. Jollet, W. Lafargue-Dit-Hauret, K. Lejaeghere, M. A. L. Marques, A. Martin, C. Martins, H. P. C. Miranda, F. Naccarato, K. Persson, G. Petretto, V. Planes, Y. Pouillon, S. Prokhorenko, F. Ricci, G.-M. Rignanese, A. H. Romero, M. M. Schmitt, M. Torrent, M. J. van Setten, B. V. Troeye, M. J. Verstraete, G. Zerah, and J. W. Zwanziger, *Comput. Phys. Commun.* **248**, 107042 (2020).
- ⁹⁷S. Poncé, E. Margine, C. Verdi, and F. Giustino, *Computer Physics Communications* **209**, 116 (2016).
- ⁹⁸L. N. Oliveira, E. K. U. Gross, and W. Kohn, *Phys. Rev. Lett.* **60**, 2430 (1988).
- ⁹⁹M. Lüders, M. A. L. Marques, N. N. Lathiotakis, A. Floris, G. Profeta, L. Fast, A. Continenza, S. Massidda, and E. K. U. Gross, *Phys. Rev. B* **72**, 024545 (2005).
- ¹⁰⁰M. A. L. Marques, M. Lüders, N. N. Lathiotakis, G. Profeta, A. Floris, L. Fast, A. Continenza, E. K. U. Gross, and S. Massidda, *Phys. Rev. B* **72**, 024546 (2005).
- ¹⁰¹A. K. Mishra, T. Muramatsu, H. Liu, Z. M. Geballe, M. Somayazulu, M. Ahart, M. Baldini, Y. Meng, E. Zurek, and R. J. Hemley, *J. Phys. Chem. C* **122**, 19370 (2018).
- ¹⁰²Z. Shao, D. Duan, Y. Ma, H. Yu, H. Song, H. Xie, D. Li, F. Tian, B. Liu, and T. Cui, *Inorg. Chem.* **58**, 2558 (2019).
- ¹⁰³J. Hooper, T. Terpstra, A. Shamp, and E. Zurek, *J. Phys. Chem. C* **118**, 6433 (2014).
- ¹⁰⁴Y. Wang, H. Wang, J. S. Tse, T. Itaka, and Y. Ma, *Phys. Chem. Chem. Phys.* **17**, 19379 (2015).
- ¹⁰⁵K. Abe, *Phys. Rev. B* **96**, 144108 (2017).
- ¹⁰⁶S. Qian, X. Sheng, X. Yan, Y. Chen, and B. Song, *Phys. Rev. B* **96**, 094513 (2017).
- ¹⁰⁷X. Ye, N. Zarifi, E. Zurek, R. Hoffmann, and N. W. Ashcroft, *J. Phys. Chem. C* **122**, 6298 (2018).
- ¹⁰⁸Y. Li, J. Hao, H. Liu, J. S. Tse, Y. Wang, and Y. Ma, *Sci. Rep.* **5**, 9948 (2015).
- ¹⁰⁹B. Li, Z. Miao, L. Ti, S. Liu, J. Chen, J. Shi, and E. Gregoryanz, *J. Appl. Phys.* **126**, 235901 (2019).

- ¹¹⁰N. P. Salke, M. M. D. Esfahani, Y. Zhang, I. A. Kruglov, J. Zhou, Y. Wang, E. Greenberg, J. Prakapenka, V. B. amd Liu, A. R. Oganov, and J.-F. Lin, *Nature Commun.* **10**, 4453 (2019).
- ¹¹¹D. Zhou, D. V. Semenov, D. Duan, H. Xie, W. Chen, X. Huang, X. Li, B. Liu, A. R. Oganov, and T. Cui, *Sci. Adv.* **6**, eaax6849 (2020).
- ¹¹²M. Peña Alvarez, J. Binns, A. Hermann, L. C. Kelsall, P. Dalladay-Simpson, E. Gregoryanz, and R. T. Howie, *Phys. Rev. B* **100**, 184109 (2019).
- ¹¹³D. V. Semenov, A. G. Kvashnin, A. G. Ivanova, V. Svitlyk, V. Y. Fominski, A. V. Sadakov, O. A. Sobolevskiy, V. M. Pudalov, I. A. Troyan, and A. R. Oganov, *Mater. Today* **33**, 36 (2020).
- ¹¹⁴D. Zhou, D. V. Semenov, H. Xie, X. Huang, D. Duan, A. Aperis, P. M. Oppeneer, M. Galasso, A. I. Kartsev, A. G. Kvashnin, A. R. Oganov, and T. Cui, *J. Am. Chem. Soc.* **142**, 2803 (2020).
- ¹¹⁵A. G. Kvashnin, D. V. Semenov, I. A. Kruglov, I. A. Wrona, and A. R. Oganov, *ACS Appl. Mater. Interfaces* **10**, 43809 (2018).
- ¹¹⁶K. Abe, *Phys. Rev. B* **98**, 134103 (2018).
- ¹¹⁷T. Bi and E. Zurek, *Chem: Eur. J.* **27**, 14858 (2021).
- ¹¹⁸R. Hoffmann and C. Zheng, *J. Phys. Chem.* **89**, 4175 (1985).
- ¹¹⁹R. Hoffmann, *Angew. Chem. Int. Ed. Engl.* **26**, 846 (1987).
- ¹²⁰D. C. Lonie, J. Hooper, B. Altintas, and E. Zurek, *Phys. Rev. B* **87**, 054107 (2013).
- ¹²¹D. V. Semenov, A. G. Kvashnin, I. A. Kruglov, and A. R. Oganov, *J. Phys. Chem. Lett.* **9**, 1920 (2018).
- ¹²²W. Chen, D. V. Semenov, X. Huang, H. Shu, X. Li, D. Duan, T. Cui, and A. R. Oganov, *Phys. Rev. Lett.* **127**, 117001 (2021).
- ¹²³X. Feng, J. Zhang, G. Gao, H. Liu, and H. Wang, *RSC Adv.* **5**, 59292 (2015).
- ¹²⁴W. Sun, X. Kuang, H. D. J. Keen, C. Lu, and A. Hermann, *Phys. Rev. B* **102**, 144524 (2020).
- ¹²⁵P. Zaleski-Ejgierd, R. Hoffmann, and N. W. Ashcroft, *Phys. Rev. Lett.* **107**, 037002 (2011).
- ¹²⁶J. Hooper and E. Zurek, *Chem. Eur. J.* **18**, 5013 (2012).
- ¹²⁷J. Hooper, B. Altintas, A. Shamp, and E. Zurek, *J. Phys. Chem. C* **117**, 2982 (2013).
- ¹²⁸C. Heil, S. di Cataldo, G. B. Bachelet, and L. Boeri, *Phys. Rev. B* **99**, 220502(R) (2019).
- ¹²⁹X. Xiao, D. Duan, H. Xie, S. Zhao, D. Li, F. Tian, H. Song, H. Yu, K. Bao, and T. Cui, *J. Phys.: Condens. Matter* **31**, 315403 (2019).
- ¹³⁰H. Liu, I. I. Naumov, Z. M. Geballe, M. Somayazulu, J. S. Tse, and R. J. Hemley, *Phys. Rev. B* **98**, 100102(R) (2018).
- ¹³¹E. R. Margine and F. Giustino, *Phys. Rev. B* **87**, 024505 (2013).
- ¹³²X. Li, X. Huang, D. Duan, C. J. Pickard, D. Zhou, H. Xie, Q. Zhuang, Y. Huang, Q. Zhou, B. Liu, and T. Cui, *Nature Commun.* **10**, 3461 (2019).
- ¹³³W. Chen, D. V. Semenov, X. Huang, H. Shu, X. Li, D. Duan, T. Cui, and A. R. Oganov, *Phys. Rev. Lett.* **127**, 117001 (2021).
- ¹³⁴H. Jeon, C. Wang, S. Yi, and J.-H. Cho, *Sci. Rep.* **10**, 16878 (2020).
- ¹³⁵Z. M. Geballe, H. Liu, A. K. Mishra, M. Ahart, M. Somayazulu, Y. Meng, M. Baldini, and R. J. Hemley, *Angew. Chem. Int. Ed.* **57**, 688 (2018).
- ¹³⁶D. Wang, H. Zhang, H.-L. Chen, J. Wu, Q.-J. Zang, and W.-C. Lu, *Phys. Lett. A* **383**, 774 (2019).
- ¹³⁷I. Errea, M. Calandra, C. J. Pickard, J. R. Nelson, R. J. Needs, Y. Li, H. Liu, Y. Zhang, Y. Ma, and F. Mauri, *Nature* **532**, 81 (2016).
- ¹³⁸B. Guigue, A. Marizy, and P. Loubeyre, *Phys. Rev. B* **102**, 014107 (2020).
- ¹³⁹X. Liang, A. Bergara, L. Wang, B. Wen, Z. Zhao, X.-F. Zhou, J. He, G. Gao, and Y. Tian, *Phys. Rev. B* **99**, 100505(R) (2019).
- ¹⁴⁰L.-T. Shi, Y.-K. Wei, A.-K. Liang, R. Turnbull, C. Cheng, X.-R. Chen, and G.-F. Ji, *J. Mater. Chem. C* **9**, 7284 (2021).
- ¹⁴¹H. Liu, R. Cheng, K. Yang, B. Li, L. Chen, and W. Lu, *Phys. Lett. A* **390**, 127109 (2021).
- ¹⁴²P. Song, Z. Hou, P. B. de Castro, K. Nakano, K. Hongo, Y. Takano, and R. Maezono, arXiv:2103.00193 (2021).
- ¹⁴³P. Song, Z. Hou, P. B. de Castro, K. Nakano, K. Hongo, Y. Takano, and R. Maezono, arXiv:2107.05498 (2021).
- ¹⁴⁴D. V. Semenov, I. A. Troyan, A. G. Ivanova, A. G. Kvashnin, I. A. Kruglov, M. Hanfland, A. V. Sadakov, O. A. Sobolevskiy, K. S. Pervakov, I. S. Lyubutin, K. V. Glazyrin, N. Giordano, D. N. Karimov, A. L. Vasiliev, R. Akashi, V. M. Pudalov, and A. R. Oganov, *Mater. Today* **48**, 18 (2021).
- ¹⁴⁵Y. Sun, J. Lv, Y. Xie, H. Liu, and Y. Ma, *Phys. Rev. B* **123**, 097001 (2019).
- ¹⁴⁶S. Di Cataldo, C. Heil, W. von der Linden, and L. Boeri, *Phys. Rev. B* **104**, L020511 (2021).
- ¹⁴⁷Z. Zhang, T. Cui, M. J. Hutcheon, A. M. Shipley, H. Song, M. Du, D. Kresin, V. and Duan, C. J. Pickard, and Y. Yao, arXiv:2106.09879 (2021).
- ¹⁴⁸M. Gao, X.-Y. Yan, Z.-Y. Lu, and T. Xiang, *Phys. Rev. B* **104**, L100504 (2021).
- ¹⁴⁹A. P. Durajski and R. Szczesniak, *Phys. Chem. Chem. Phys.*, Accepted Manuscript (2021).
- ¹⁵⁰C. Kokail, W. von der Linden, and L. Boeri, *Phys. Rev. Mater.* **1**, 074803 (2017).
- ¹⁵¹S. Di Cataldo, W. von der Linden, and L. Boeri, *Phys. Rev. B* **102**, 014516 (2020).
- ¹⁵²S. Di Cataldo, W. von der Linden, and L. Boeri, arXiv:2106.07266 (2021).
- ¹⁵³X. Liang, A. Bergara, X. Wei, L. Wang, R. Sun, H. Liu, R. J. Hemley, L. Wang, G. Gao, and Y. Tian, *Phys. Rev. B* **104**, 134501 (2021).
- ¹⁵⁴B. Liu, W. Cui, J. Shi, J. Zhu, J. Chen, S. Lin, R. Su, J. Ma, K. Yang, M. Xu, J. Hao, A. P. Durajski, J. Qi, Y. Li, and Y. Li, *Phys. Rev. B*, 174101 (2018).
- ¹⁵⁵Y. Ge, F. Zhang, and Y. Yao, *Phys. Rev. B*, 224513 (2016).
- ¹⁵⁶Y. Ge, F. Zhang, R. P. Dias, R. J. Hemley, and Y. Yao, *Mater. Today Phys.* **15**, 100330 (2020).
- ¹⁵⁷Y. Sun, Y. Tian, B. Jiang, X. Li, H. Li, Y. Iitaka, X. Zhong, and Y. Xie, *Phys. Rev. B* **101**, 174102 (2020).

- ¹⁵⁸W. Cui, T. Bi, J. Shi, Y. Li, H. Liu, E. Zurek, and R. J. Hemley, *Phys. Rev. B* **101**, 134504 (2020).
- ¹⁵⁹Y. Yan, T. Bi, N. Geng, X. Wang, and E. Zurek, *J. Phys. Chem. Lett.*, 9629 (2020).
- ¹⁶⁰F. Tian, D. Li, X. Sha, Y. Liu, T. Yang, B. Liu, and T. Cui, *Mater. Res. Express* **2**, 046001 (2015).
- ¹⁶¹X. Li, Y. Xie, Y. Sun, P. Huang, H. Liu, C. Chen, and Y. Ma, *J. Phys. Chem. Lett.* **11**, 935 (2020).
- ¹⁶²Y. Liu, Y. Sun, and P. Gao, *Solid State Commun.* **329**, 114260 (2021).
- ¹⁶³S. X. Hu, R. Paul, V. V. Karasiev, and R. P. Dias, *arXiv:2012.10259* (2020).
- ¹⁶⁴J. E. Hirsch and F. Marsiglio, *Nature* **596**, E9 (2021).
- ¹⁶⁵M. Dogan and M. L. Cohen, *Phys. C: Superconductivity and its Applications* **583**, 1353851 (2021).
- ¹⁶⁶T. Wang, M. Hirayama, T. Nomoto, T. Koretsune, R. Arita, and J. A. Flores-Livas, *Phys. Rev. B* **104**, 064510 (2021).
- ¹⁶⁷H. Guan, Y. Sun, and H. Liu, *arXiv:2108.09437* (2021).
- ¹⁶⁸X. Wang, T. Bi, K. P. Hilleke, A. Lamichhane, R. J. Hemley, and E. Zurek, *arXiv:2109.09898* (2021).
- ¹⁶⁹E. Bykova, M. Bykov, S. Chariton, V. B. Prakapenka, K. Glazyrin, A. Aslandukov, A. Aslandukova, G. Criniti, A. Kurnosov, and A. F. Goncharov, *Phys. Rev. B* **103**, L140105 (2021).
- ¹⁷⁰A. Lamichhane, R. Kumar, M. Ahart, N. P. Salke, N. Dasenbrock-Gammon, E. Snider, Y. Meng, B. Lavina, S. Chariton, V. B. Prakapenka, M. Somayazulu, R. P. Dias, and R. J. Hemley, *J. Chem. Phys.* **155**, 114703 (2021).
- ¹⁷¹Y. Ma, D. Duan, Z. Shao, H. Yu, H. Liu, F. Tian, X. Huang, D. Li, B. Liu, and T. Cui, *Phys. Rev. B* **96**, 144518 (2017).
- ¹⁷²Y. Ma, D. Duan, Z. Shao, D. Li, L. Wang, H. Yu, F. Tian, H. Xie, B. Liu, and T. Cui, *Phys. Chem. Chem. Phys.* **19**, 27406 (2017).
- ¹⁷³X. Song, K. Yin, Y. Wang, A. Hermann, H. Liu, J. Lv, Q. Li, C. Chen, and Y. Ma, *J. Phys. Chem. Lett.* **10**, 2761 (2019).
- ¹⁷⁴K. Tanaka, J. S. Tse, and H. Liu, *Phys. Rev. B* **96**, 100502(R) (2017).
- ¹⁷⁵L. Zhang, Y. Wang, J. Lv, and Y. Ma, *Nature Rev. Mater.* **2**, 17005 (2017).
- ¹⁷⁶C. Toher, C. Oses, D. Hicks, and S. Curtarolo, *npj Comput. Mater.* **5**, 69 (2019).
- ¹⁷⁷V. L. Deringer, D. M. Proserpio, G. Csányi, and C. J. Pickard, *Faraday Discuss.* **211**, 45 (2018).
- ¹⁷⁸V. L. Deringer, C. J. Pickard, and G. Csányi, *Phys. Rev. Lett.* **120**, 156001 (2018).